RhoA GTPase inhibition organizes contraction during epithelial morphogenesis

Frank M. Mason,[1] Shicong Xie,[2] Claudia G. Vasquez,[1] Michael Tworoger,[1] and Adam C. Martin[1]

[1]Department of Biology and [2]Computational and Systems Biology, Massachusetts Institute of Technology, Cambridge, MA 02142

During morphogenesis, contraction of the actomyosin cytoskeleton within individual cells drives cell shape changes that fold tissues. Coordination of cytoskeletal contractility is mediated by regulating RhoA GTPase activity. Guanine nucleotide exchange factors (GEFs) activate and GTPase-activating proteins (GAPs) inhibit RhoA activity. Most studies of tissue folding, including apical constriction, have focused on how RhoA is activated by GEFs to promote cell contractility, with little investigation as to how GAPs may be important. Here, we identify a critical role for a RhoA GAP, Cumberland GAP (C-GAP), which coordinates with a RhoA GEF, RhoGEF2, to organize spatiotemporal contractility during *Drosophila melanogaster* apical constriction. C-GAP spatially restricts RhoA pathway activity to a central position in the apical cortex. RhoGEF2 pulses precede myosin, and C-GAP is required for pulsation, suggesting that contractile pulses result from RhoA activity cycling. Finally, C-GAP expression level influences the transition from reversible to irreversible cell shape change, which defines the onset of tissue shape change. Our data demonstrate that RhoA activity cycling and modulating the ratio of RhoGEF2 to C-GAP are required for tissue folding.

Introduction

Cell and tissue shape changes require force generation via the F-actin and nonmuscle myosin-II (myosin) cytoskeleton, which forms the cortex that lines the plasma membrane and is coupled to adhesion molecules, such as E-cadherin (E-cad; Salbreux et al., 2012; Vasquez and Martin, 2016). F-Actin and myosin structures that promote epithelial cell shape changes have been shown to be dynamic and spatially organized (Blanchard et al., 2010; He et al., 2010; Rauzi et al., 2010; Levayer et al., 2011; Mason et al., 2013; Kasza et al., 2014; Vasquez et al., 2014; Jodoin et al., 2015; Munjal et al., 2015). F-actin and myosin assembly are regulated by the Rho family of GTPases, molecular switches that bind GTP, localize to the plasma membrane, and activate downstream effectors (Jaffe and Hall, 2005). Two families of proteins catalyze the cycling between inactive and active states: guanine nucleotide exchange factors (GEFs) and GTPase-activating proteins (GAPs; Bos et al., 2007). Previous work has identified GEFs that activate RhoA at particular times in development (Barrett et al., 1997; Häcker and Perrimon, 1998; Schumacher et al., 2004; Smallhorn et al., 2004; Simões et al., 2006; Nakaya et al., 2008; Levayer et al., 2011; Nishimura et al., 2012), yet less is known about the role of GAPs during morphogenesis.

One well-studied example where RhoA activation leads to tissue morphogenesis is epithelial folding during *Drosophila* embryogenesis. One RhoA GEF, RhoGEF2, promotes numerous folding events in the *Drosophila melanogaster* embryo (Barrett et al., 1997; Häcker and Perrimon, 1998; Dawes-Hoang et al., 2005; Grosshans et al., 2005; Simões et al., 2006; Fox and Peifer, 2007). In one of these folding events, ventral furrow formation, a group of ∼1,000 epithelial cells undergoes apical constriction. Apical constriction changes columnar cells to a wedge-shape, which facilitates epithelial bending (Sawyer et al., 2010; Martin and Goldstein, 2014). The ventral furrow is specified by the transcription factors Snail and Twist, which activate expression of several factors, including a G protein–coupled receptor pathway, that ultimately promotes the apical accumulation of RhoGEF2 (Leptin, 1991; Costa et al., 1994; Fox and Peifer, 2007; Kölsch et al., 2007; Manning et al., 2013; Kerridge et al., 2016). It is thought that apical RhoGEF2 activates the RhoA pathway to stimulate apical constriction. Whether RhoA activation is sufficient to promote apical constriction is unknown.

Myosin contractility exhibits spatial and temporal organization in the apical cortex (Mason et al., 2013; Kasza et al., 2014; Vasquez et al., 2014; Munjal et al., 2015; Xie and Martin, 2015). Myosin undergoes discrete accumulations, or pulses, that correlate with apical constriction (Martin et al., 2009; Xie and Martin, 2015). The RhoA effector Rho-associated and coiled-coil kinase (ROCK; Rok in *Drosophila*) also exhibits pulses (Vasquez et al., 2014; Munjal et al., 2015); because ROCK activates myosin and myosin phosphatase is required for pulsing, pulses likely reflect cyclical activation of myosin

Correspondence to Adam C. Martin: acmartin@mit.edu

Abbreviations used: CA, constitutively active; E-cad, E-cadherin; HF, heat fixed; MBS, myosin-binding subunit; OE, overexpression; RCP, radial cell polarity; ROCK, Rho-associated and coiled-coil kinase; WT, wild type.

The Rockefeller University Press $30.00
J. Cell Biol. Vol. 214 No. 5 603–617
www.jcb.org/cgi/doi/10.1083/jcb.201603077

motors (Vasquez et al., 2014; Munjal et al., 2015) and possibly F-actin assembly (Mason et al., 2013). These myosin pulses result in contraction of the apical F-actin network (Martin et al., 2009; Mason et al., 2013) and may promote the spatiotemporal organization of the RhoA pathway via cortical flows or advection (Munro et al., 2004; Munjal et al., 2015). In addition to temporal modulation of myosin activity, we recently demonstrated that there is a spatial organization of RhoA (Rho1 in *Drosophila*) and its effectors within the apical domain (Mason et al., 2013). ROCK is concentrated in the middle of the apical domain (medioapical) and is depleted from adherens junctions, a distribution termed radial cell polarity (RCP; Mason et al., 2013; Xie and Martin, 2015). RCP is dependent on Twist, but the molecules, and thus the mechanisms, that polarize RhoA activity in the apical cortex are not known.

Here, we discovered that RhoA activation is required for, but not sufficient to, promote medioapical ROCK/myosin accumulation and apical constriction. RhoGEF2 pulses can precede myosin accumulation, suggesting that RhoA activation initiates contractile pulses. We identified a Rho GAP that we named Cumberland GAP (C-GAP), which regulates both the spatial and temporal activation of RhoA. We found that C-GAP is critical for myosin pulsing and that C-GAP levels dictate whether cell shape changes are reversible or irreversible, like a ratchet. Collectively, our data demonstrate that simply turning on RhoA activity does not promote apical constriction. Instead, RhoA GTPase cycling by a paired RhoGEF2–C-GAP module is required for apical constriction and modulating the ratio of GEF to GAP over time is critical for ratchet-like contractions associated with proper tissue folding.

Results

Constitutive RhoA activation does not stimulate apical constriction

During ventral furrow cell apical constriction, the RhoA activator RhoGEF2 is required for apical localization of myosin, but it is unknown whether RhoA activity itself is required or sufficient for ventral furrow formation (Dawes-Hoang et al., 2005; Fox and Peifer, 2007). *rho1* mutants do not proceed to gastrulation, and inhibition of RhoA activity perturbs earlier developmental processes, including cellularization (Crawford et al., 1998; Magie et al., 1999). Thus, to test whether RhoA activity is required for apical ROCK and myosin activity during apical constriction, we acutely inhibited RhoA activity by injecting the C3-exoenzyme RhoA inhibitor during ventral furrow formation (Crawford et al., 1998). The C3 inhibitor prevented apical accumulation of both ROCK and myosin (Fig. 1, A and B). Additionally, C3 injection into embryos that have already initiated apical constriction resulted in a loss of myosin, suggesting that sustained RhoA activity is required to maintain apical ROCK/myosin throughout ventral furrow formation (Fig. S1 A). These data demonstrate that RhoA activity is absolutely necessary for ROCK and myosin apical localization.

In many cell types, overexpression (OE) of constitutively active RhoA promotes stress fiber formation and cell contractility (Ridley and Hall, 1992; Tojkander et al., 2012; Burridge and Wittchen, 2013). As apical constriction in ventral furrow cells also requires the formation of myosin fibers (Martin et al., 2010), we asked whether active RhoA is sufficient to promote medioapical myosin fiber formation and apical constriction. To test this, we expressed constitutively active (CA) RhoA (G14V) and quantified apical constriction as well as localization and dynamics of myosin. We injected embryos with CA-RhoA mRNA at one pole to generate a gradient of CA-RhoA expression. We observed that CA-RhoA stimulates more apical myosin accumulation in cells proximal to the injection, as well as more gradual myosin accumulation, without obvious myosin pulsing (Fig. 1, C and D; and Fig. S1 B). In contrast to cells distal to the injection (and wild-type [WT] cells, not shown), myosin initially accumulates at the junctions instead of the medioapical cortex where CA-RhoA is overexpressed, as indicated by a lower medioapical/junctional ratio of apical myosin (Fig. 1, C and E). Cells distal to the CA-RhoA injection were able to constrict their apical surface and the ventral furrow invaginated (Fig. 1, C and F). In contrast, proximal cells that have mislocalized myosin failed to collectively constrict and invaginate (Fig. 1, C and F). Overexpression of WT-RhoA did not induce ectopic accumulation of myosin (Video 1), suggesting that the activity, but not the amount, of RhoA promotes myosin organization. These results demonstrated that active RhoA is necessary, but not sufficient, for proper myosin organization in the ventral furrow. Also, simply turning RhoA "on" is insufficient for proper epithelial contractility, which implied that regulation and potentially activity cycling of RhoA is critical to organize RhoA pathway activity.

Apical RhoGEF2 pulses precede myosin pulses

To understand how apical RhoA is activated to promote radially polarized and pulsatile ROCK/myosin, we determined the spatiotemporal dynamics of one of RhoA's activators, RhoGEF2. Previous work in fixed tissues showed that RhoGEF2 is recruited apically and required for apical recruitment of myosin (Dawes-Hoang et al., 2005; Fox and Peifer, 2007; Kölsch et al., 2007). Fixing embryos in a manner that preserved the apical actin cortex confirmed that endogenous RhoGEF2 was apically enriched, present at cell–cell boundaries and colocalized with medioapical myosin (Fig. 2, A and B). However, the temporal dynamics of RhoGEF2 were unknown. Therefore, we constructed a GFP-tagged RhoGEF2 (GFP::RhoGEF2) that is expressed from the endogenous RhoGEF2 promoter, using recombineering of a bacterial artificial chromosome (Venken et al., 2009). GFP::RhoGEF2 rescued *rhogef2* mutants, demonstrating that GFP::RhoGEF2 functionally substitutes for the endogenous RhoGEF2 (see Materials and methods).

GFP::RhoGEF2 in live tissues also strongly colocalized with medioapical myosin during later stages of ventral furrow invagination and was planar polarized in the lateral tissues of the germband (Fig. 2 C and Fig. S2 B), consistent with staining in fixed germband tissues (Levayer et al., 2011). Interestingly, we only observed junctional GFP::RhoGEF2 at subapical positions in live tissues or in fixed samples (Fig. S2 A). This suggested that junctional RhoGEF2 may be less abundant than medioapical RhoGEF2, that fixation may reduce medioapical RhoGEF2 levels, or that the GFP tag might alter RhoGEF2 localization. We also observed that RhoGEF2 levels increased throughout ventral furrow formation, suggesting that apical RhoA activity increases during invagination (Fig. 2 D). Moreover, we observed clear pulsatile accumulations of RhoGEF2 in constricting cells in early stages of invagination (Fig. 2 E). During these early pulses, RhoGEF2 appears to fill the entire apical cortex. We then asked how RhoGEF2 pulses are temporally coordinated

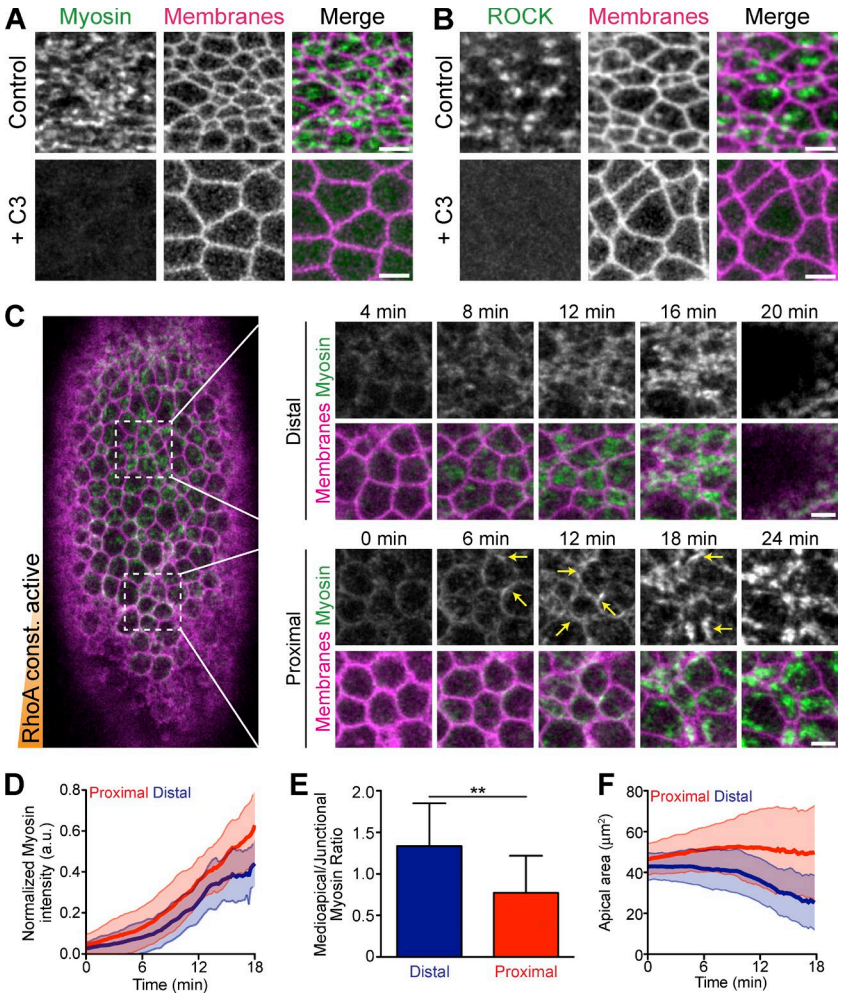

Figure 1. **Constitutively active RhoA is insufficient for apical constriction.** (A) Apical myosin depends on RhoA activity. Images from live embryos expressing myosin::GFP (sqh::GFP) and membrane::RFP (Gap43::mCherry) and injected with buffer (PBS, Control) or the C3 exoenzyme immediately before gastrulation. (B) Apical ROCK localization depends on RhoA activity. Images from live embryos expressing GFP::ROCK and Membrane::RFP injected with solvent or C3 immediately before gastrulation. (C) Constitutively active RhoA (CA-RhoA) disrupts proper myosin organization in ventral furrow cells. Image of a live embryo expressing Myosin::GFP and Membrane::RFP that has been injected at one pole (bottom) with mRNA encoding CA-RhoA (G14V). Time-lapse images (right) show myosin accumulating abnormally at junctions (arrows), specifically in cells proximal to injection. (D) Quantification of total apical myosin intensity in embryo in C injected with CA-RhoA mRNA (n = 47 cells proximal, 44 cells distal from two embryos; error bars represent ±SD). Note that myosin intensity is slightly higher close to the injection site (proximal). a.u., arbitrary units. (E) Quantification of myosin intensity in the middle of the apical surface (medioapical) relative to the junctions. Cells proximal to CA-RhoA injection have a lower medioapical-to-junctional ratio (n = 12 cells proximal, 12 cells distal; **, $P < 0.01$, unpaired t test; error bars represent ±SD). (F) Apical constriction is impaired in cells proximal to CA-RhoA injection (n = 47 cells proximal, 44 cells distal; error bars represent ±SD). Bars, 5 µm.

with myosin pulses. Pulse behavior was heterogeneous (Fig. S2 C and Video 2); RhoGEF2 pulses did co-occur with myosin pulses, but peak RhoGEF2 intensity frequently preceded the peak of the myosin intensity by 10.4 ± 7 s (n = 187 pulses, 5 embryos; Fig. 2, F and G). Because the peak of the myosin and ROCK pulse occurred simultaneously (Vasquez et al., 2014; Munjal et al., 2015), this result suggested that the appearance of RhoGEF2 precedes RhoA/ROCK activation. Overall, our data suggested that pulses of RhoGEF2, and thus RhoA activity, result in pulsatile ROCK and myosin accumulation.

Identification of a Rho GAP that is critical for epithelial folding

Our data showed that simply expressing active RhoA is not sufficient to promote normal myosin organization required for apical constriction. Therefore, we hypothesized that inactivation by an unidentified Rho GAP may be a critical component of this contractile system. RhoA inactivation by a GAP may turn off RhoA between RhoGEF2 pulses and influence pulsatile ROCK/myosin. We also hypothesized that a GAP might spatially organize the RhoA–ROCK–myosin pathway, promoting RCP.

We screened all 22 *Drosophila* Rho GAPs to identify a single GAP, RhoGAP71E, which is critical for ventral furrow formation (see Materials and methods and Table S1). Although little is known about RhoGAP71E during epithelial morphogenesis (Greenberg and Hatini, 2011), it regulates RhoA activity levels and cell shape changes in cultured insect cells (Bakal et al., 2007; Sailem et al., 2014). *rhogap71e* mRNA is maternally loaded, and is enriched ventrally and in the cephalic furrow during gastrulation (Fig. 3 A). RhoGAP71E protein is apically localized and colocalizes with myosin, specifically in the ventral furrow, similar to RhoGEF2 (Fig. 3, B and C). Across the apical surface, RhoGAP71E localizes to cell–cell junctions and forms medioapical structures that localize with myosin (Fig. 3 D). Because *rhogap71e* is expressed in the embryonic furrows (Fig. 3, A and B), we named it Cumberland GAP (C-GAP) after the passage or gap in the Appalachian Mountains. In addition, loss of C-GAP resulted in abnormal furrow shape, resulting in a C-shaped, rather than V-shaped, ventral furrow (Fig. 3 E). Thus, the name C-GAP also reflects the mutant phenotype of the ventral furrow.

In cultured cells, OE of RhoA GAPs can suppress formation of actomyosin stress fibers by decreasing RhoA activity (Ridley et al., 1993; Vincent and Settleman, 1999; Krugmann et al., 2002; Miura et al., 2002; Wennerberg et al., 2003; Yeung et al., 2014). Therefore, to test whether C-GAP function is consistent with a RhoA GAP, we overexpressed C-GAP (via capped mRNA injections) and asked whether this lowered apical myosin and Rho-GTP levels (Fig. 3, F and G). In control (H_2O-injected) embryos, apical myosin formed a fibrous network spanning across the apical surface (Fig. 3 F). However, OE of C-GAP blocked apical myosin accumulation. To test whether the GAP activity is required to suppress apical myosin, we mutated the arginine finger (R77A) required for GTPase activity or deleted the

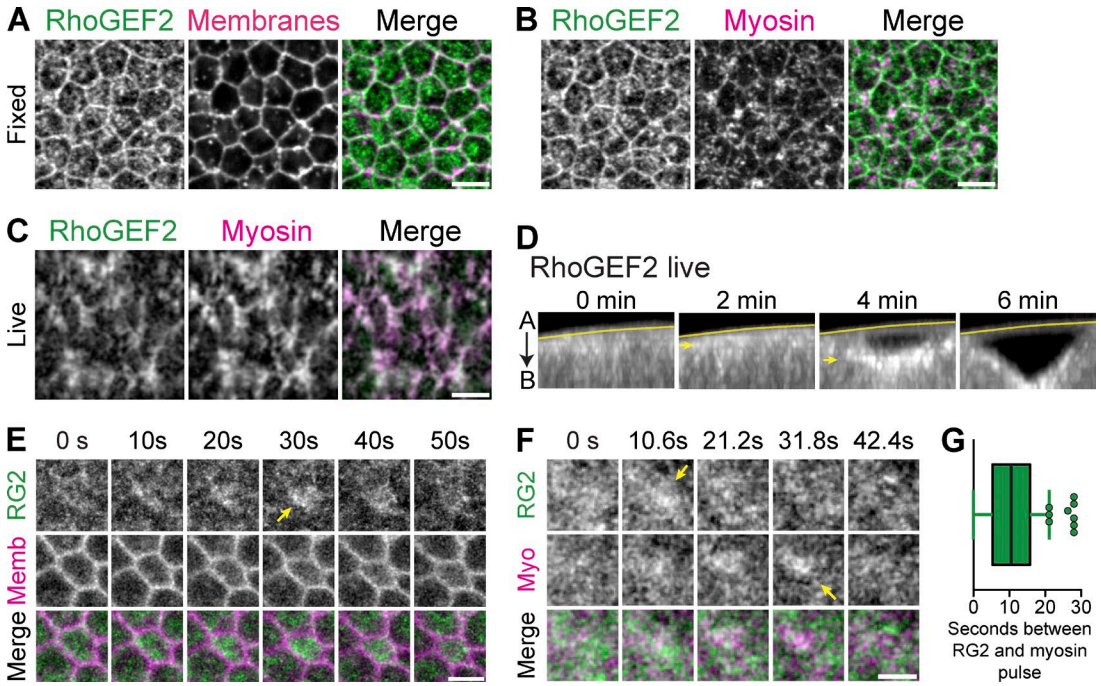

Figure 2. **Medioapical RhoGEF2 pulses precede ROCK-myosin.** (A–C) RhoGEF2 localizes across the medioapical surface. (A and B) Images from fixed Myosin::GFP (*sqh*::GFP) embryos, stained with a RhoGEF2 antibody. Membranes are subapical F-actin (phalloidin). (C) Images from live embryos expressing GFP::RhoGEF2 and myosin::RFP. Note the strong colocalization of RhoGEF2 with myosin. (D) Images of cross section views of ventral furrow formation in live embryos showing increasing apical accumulation of GFP::RhoGEF2 (arrows). Line marks the vitelline membrane. (E) Time-lapse images represent apical GFP::RhoGEF2 and subapical membrane::RFP. Pulses of RhoGEF2 occur across the entire medioapical region (arrow). (F) Time-lapse images of embryo expressing GFP::RhoGEF2 and myosin::RFP show pulsed accumulation (arrows). (G) Quantifications of time delay, in seconds, between RhoGEF2 and myosin pulses (mean = 10.4 ± 7 s, *n* = 187 pulses, 5 embryos; error bars represent SD). Bars: (A–C) 5 µm; (E and F) 2.5 µm.

GAP domain from full-length C-GAP. Overexpression of either the R77A mutant or the GAP deletion mutant did not suppress myosin accumulation (Fig. 3 F). In addition, we tested whether C-GAP OE affected apical RhoA-GTP activity using a biosensor for RhoA-GTP (anillin Rho-binding domain [AniRBD::GFP]; Piekny and Glotzer, 2008; Munjal et al., 2015). Overexpression of C-GAP decreased apical AniRBD accumulation, similar to Rho inhibition with C3, in a manner dependent on the GAP domain (Fig. 3 G). Although we cannot rule out that C-GAP may regulate other Rho-family GTPases, our results indicate that the GAP domain of C-GAP antagonizes the RhoA pathway.

C-GAP is required for RCP of the apical cortex and tissue folding

During apical constriction, ventral furrow cells exhibit a meshwork of myosin fibers, with myosin being most concentrated near the center of the apical domain. Furthermore, ROCK is present in a concentrated medioapical focus, and ROCK intensity drops off around the cell circumference near the junctional domain, defining an RCP of the apical cortex (Mason et al., 2013). We examined the apical organization of myosin and ROCK in both *C-GAP shRNA* and genetic mutant embryos (Fig. 4, A–D). To disrupt *C-GAP* expression, *C-GAP shRNA* was maternally loaded using the UAS-GAL4 system, or *C-GAP* germline mutant clones were generated (Chou and Perrimon, 1992; Perkins et al., 2015). In both cases, depletion of maternal C-GAP resulted in several classes of phenotypes. In some cases, C-GAP depletion disrupted cellularization, and furrow canals prematurely constricted, causing nuclei to be squeezed or remain in the yolk (Fig. S3, A and C). Whereas myosin in furrow canals moved basally toward the yolk in *control* (*white*) *shRNA*, basal movement of the cellularization front is halted prematurely in *C-GAP shRNA* embryos (Fig. S3 B). Apical myosin appears in the ventral furrow with normal developmental timing (around the time of cephalic furrow formation), despite the fact that cellularization is disrupted (Fig. S3 B).

C-GAP–depleted embryos were also observed that proceeded through cellularization and exhibited two classes of phenotypes we termed mild and severe based on whether ventral furrow invagination is delayed or blocked (Fig. 4, A and C–H; and Videos 3–5). We classified C-GAP–depleted embryos with delayed furrow invagination as having a "mild" phenotype. C-GAP–depleted embryos that did not invaginate, despite apical ROCK/myosin accumulation, were classified as "severe" (Video 5). Myosin typically formed nodes or fibers spanning the medioapical domain in *control shRNA*, whereas *C-GAP shRNA* embryos with mild phenotypes have diffuse myosin spread across the apical surface (Fig. 4, A and B; and Videos 3 and 4). In control embryos, ROCK is normally concentrated into one medioapical focus per cell; however, ROCK spread across the apical surface in *C-GAP shRNA* and mutant embryos with mild furrow phenotypes (Fig. 4, C and D). Interestingly, *C-GAP* depletion leads to more diffuse ROCK/myosin, a phenotype that did not completely resemble the CA-RhoA, which resulted in more junctional myosin (Fig. 1). We hypothesized this disparity is because CA-RhoA would signal to activate effectors independently from RhoGEF2, whereas C-GAP depletion would lead to excessive activation of RhoA through RhoGEF2. And as RhoGEF2 localized predominately to the medioapical cortex (Fig. 2, C, E, and F), loss of the GAP that balances RhoGEF2 could lead to excessive medioapical RhoA activity and more diffuse or spread out ROCK and myosin.

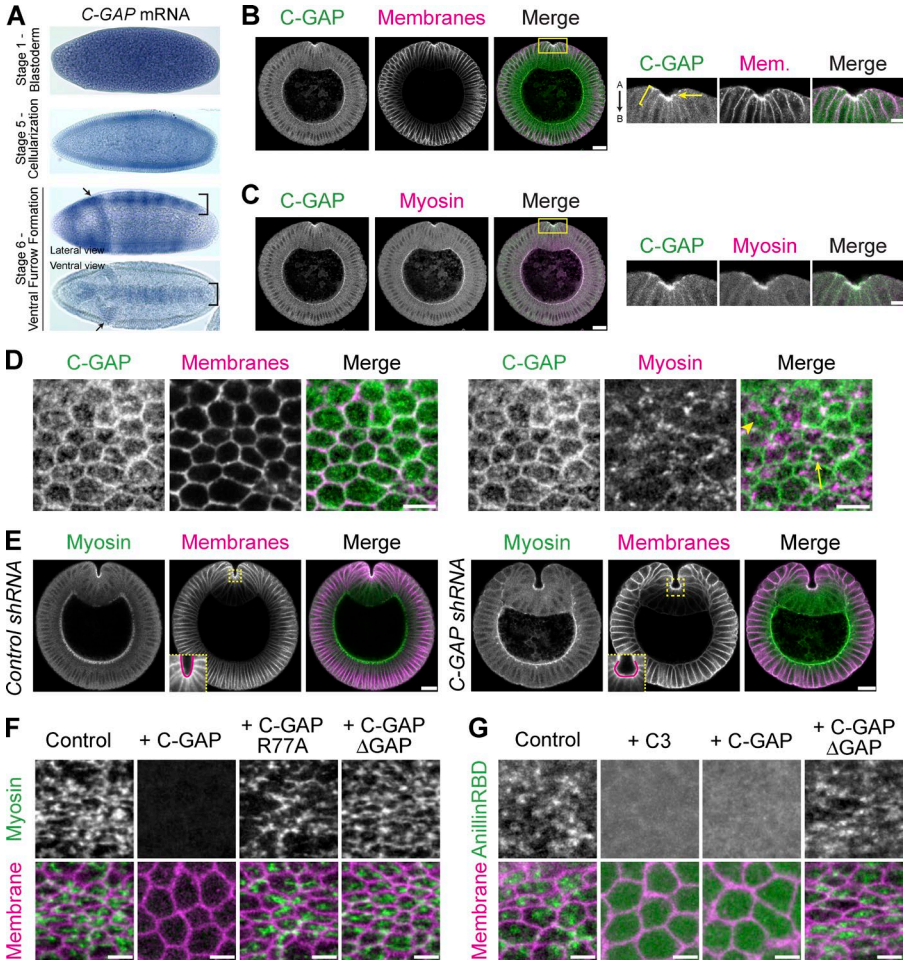

Figure 3. **Identification of a RhoA GAP, Cumberland GAP, involved in tissue folding.** (A) In situs of C-GAP mRNA. C-GAP mRNA is maternally loaded and enriched in ventral (bracket) and cephalic (arrows) furrows. (B and C) C-GAP is apically enriched (arrow) in the ventral furrow, and localizes along subapical/basolateral membranes (brackets). Images from fixed embryo, cross sections stained for C-GAP::3xHA (HA epitope), and membranes (neurotactin) or myosin (zipper). Images on right represent magnified regions from images on left (yellow boxed regions). "A" is apical and "B" is basal. (D) C-GAP localizes across the apical surface. Images from fixed myosin::GFP (*sqh*::GFP) embryos, stained for C-GAP::3xHA (HA) and with phalloidin (subapical F-actin, membranes). C-GAP forms medioapical structures with (arrow) and without (arrowhead) myosin. (E) Images from fixed *Control* (*white*) and *C-GAP shRNA* cross sectioned embryos, stained for myosin (zipper) and membranes (neurotactin). Ventral furrow in *Control* forms in a V-shape, but *C-GAP shRNA* ventral furrow is abnormally shaped, forming a cup, or C-shape (insets at bottom left of membrane channel are from boxed, yellow region). (F) C-GAP overexpression decreases apical myosin accumulation. Images from live embryos expressing myosin::GFP and membrane::RFP, injected with mRNA encoding full-length C-GAP, C-GAP with GAP mutant (R77A), C-GAP with GAP domain deletion, or control (water injection). (G) C-GAP overexpression decreases apical RhoA-GTP. Images from live embryos expressing Rho-GTP biosensor (AniRBD::GFP) and membrane::RFP and injected with PBS buffer (control), C3, or mRNA encoding full-length C-GAP or C-GAP with a GAP domain deletion. Bars: (B and C [right], D, F, and G) 5 µm; (B and C [left] and E) 20 µm.

For C-GAP–depleted embryos with severe phenotypes, ROCK/myosin becomes highly condensed into a focus and cells become less hexagonal and more rounded (Fig. 4, A, C, and D, severe; and Video 5), suggesting a defect in cell adhesion. When cells lose mechanical connections to their neighbors, the actomyosin network contracts inward without restraint, resulting in a highly condensed bolus of myosin and other apical markers (i.e., E-cad; Martin et al., 2010). Therefore, we investigated E-cad localization in C-GAP–depleted embryos. Normally, ROCK is concentrated near the center of the apical domain, and E-cad is enriched in a complementary pattern around the cell junctions (Mason et al., 2013). We found that C-GAP depletion disrupted E-cad localization, causing E-cad to spread across the apical surface (Fig. 4, E and F). Because both ROCK and E-cad are affected, we cannot conclude whether the dysregulation of contractility, adhesion, or both contribute to the loss of RCP. Additionally, the altered RhoA activity observed in *C-GAP shRNA* embryos could affect other RhoA effectors such as Diaphanous, which regulates F-actin dynamics and contributes to E-cad localization (Mason et al., 2013). Although myosin contractility prevents cell junction disassembly in the ventral furrow (Weng and Wieschaus, 2016), it is unclear whether and how perturbed contractility enables E-cad to localize across the surface. Despite this unanswered question, our results clearly show that C-GAP is required for the RCP of both ROCK/myosin, which normally localized to a medioapical focus during apical constriction, and E-cad, which is normally enriched at the apical margin. Additionally, ventral furrow cells lost basal myosin and basally expanded, and planar polarized myosin was not affected nor was there ectopic myosin in the lateral (germband) cells in *C-GAP shRNA* embryos (Fig. S4). This suggested the C-GAP depletion phenotypes are primarily caused by the requirement of C-GAP to organize apical contractility in ventral furrow cells and not ectopic contractility in other tissues or on the cells' basal surface (Polyakov et al., 2014; Rauzi et al., 2015).

ROCK and myosin localization is restricted to the apical cortex (Mason et al., 2013; Vasquez et al., 2014). However, after C-GAP depletion (via *shRNA* and germline clone mutants), ROCK localized along the basolateral cell surfaces (Fig. 4, G and H). Collectively, our results demonstrate that inhibition of RhoA activity via C-GAP is required to restrict ROCK/myosin activity to and within the apical domain.

C-GAP is required for myosin and ROCK pulsing

Wild-type ventral furrow cells exhibit ROCK and myosin pulses, in which apical myosin intensity increases and then decreases (Vasquez et al., 2014; Xie and Martin, 2015). We asked whether C-GAP also regulated pulsatile contractions. We imaged myosin and membranes in WT, *C-GAP shRNA*, and C-GAP OE embryos (Fig. S4 C), and we measured the intensity of apical myosin in individual cells. In contrast to WT and C-GAP OE cells, which exhibit pulses, *C-GAP shRNA* cells exhibited a more continuous increase in myosin (Fig. 5 A and Videos 3, 4, and 6). To quantify

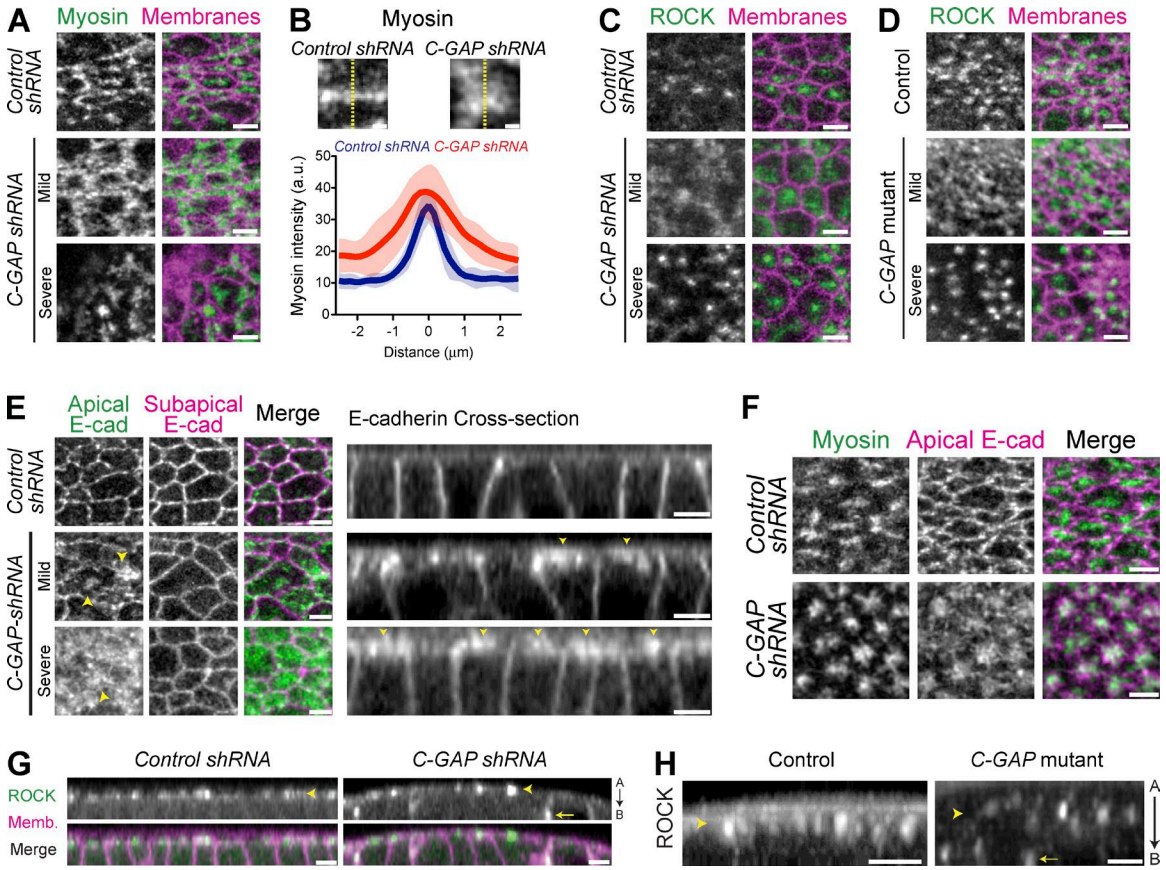

Figure 4. **C-GAP promotes spatial organization of apical RhoA pathway signaling.** (A) Images from live *control* (*white shRNA*) or *C-GAP shRNA* embryos expressing myosin::GFP and membrane::RFP. Whereas control embryos form myosin fibers or nodes spanning the apical surface, *C-GAP shRNA* embryos with mild ventral furrow phenotypes have diffuse myosin spread across the apical surface or highly condensed myosin in severe phenotypes, resembling cells that lose adhesion. (B) Linescans across myosin structures within individual cells in *Control* (n = 20) or *C-GAP shRNA* (n = 25) reveal that myosin forms less condensed or organized structures in *C-GAP shRNA* embryos (shaded areas represent ±SD). (C) Images from live *control* or *C-GAP shRNA* embryos expressing GFP::ROCK and membrane::RFP. Instead of one condensed ROCK focus in each *control* cell, *C-GAP shRNA* results in a more diffuse ROCK (mild) spreading across the entire apical domain, or highly condensed ROCK (severe), where the furrow ultimately falls apart and does not invaginate. (D) Images from live control (*C-GAP* heterozygous mutant) and *C-GAP* homozygous, germline mutant embryos expressing GFP::ROCK and membrane::RFP. Both control and *C-GAP* mutant embryos have identical ROCK localization phenotypes to *shRNA* embryos. (E and F) Images from live embryos expressing E-cadherin::GFP and myosin::RFP. (E) Apical E-cad localization is restricted to cell-cell contacts in *control shRNA* embryos, but E-cad spreads across the apical surface (arrowheads) in *C-GAP shRNA*. (F) E-cad becomes condensed with concentrated myosin structures in severe *C-GAP shRNA* embryos that appear to lose adhesion. (G) Cross sections from live embryos expressing GFP::ROCK and Membrane::RFP demonstrating C-GAP restricts ROCK activity to apical domain. In *control shRNA* embryos, ROCK localization is restricted to the apical cortex, but *C-GAP shRNA* embryos have both apical (arrowhead) and some basolateral (arrow) accumulation of ROCK. "A" is apical and "B" is basal. (H) Cross sections from live embryos expressing GFP::ROCK showing that *C-GAP* mutant embryos also have some basolateral accumulation of ROCK. Bars: (B) 1 µm; (A and C–H) 5 µm.

whether C-GAP regulated contractile pulses, we measured the occurrence of higher-magnitude constriction events in WT, *C-GAP shRNA*, and OE embryos (Fig. 5 B). We observed that although WT and C-GAP–overexpressing cells have comparable pulsing frequencies, *C-GAP shRNA* led to significantly fewer pulsing events. Additionally, the maximum constriction rate of cells in *C-GAP shRNA* embryos was significantly lower than in WT or C-GAP OE embryos (Fig. 5 C). These data demonstrate that regulation of RhoA activity, via C-GAP, is necessary for pulsing.

Interestingly, although C-GAP OE embryos exhibited pulsatile myosin and cell contraction, the amount of myosin remaining after a pulse, which we defined as the myosin persistence, was significantly decreased (Fig. 5, A and D). Myosin persistence was calculated as the normalized difference in myosin intensity between the before-peak and after-peak minimum intensity during a contraction pulse (Xie and Martin, 2015). Thus, GAP OE does not affect pulse frequency but decreases the persistence of myosin after the pulse.

Myosin pulses in *Drosophila* germband cells were recently proposed to result from a feedback loop in which myosin recruits ROCK by advection (Munjal et al., 2015). Because myosin pulses are abnormal in the C-GAP–depleted embryos, this suggested that active RhoA regulation is involved in pulsing. To test whether RhoA activity/ROCK pulsing is dependent myosin pulses, we asked whether ROCK pulses occur in cells that lack pulsatile myosin (myosin-binding subunit [MBS] of the myosin phosphatase–depleted embryos [*MBS shRNA*]; Fig. 5 E; Vasquez et al., 2014; Munjal et al., 2015). Consistent with C-GAP being required for myosin pulsing, ROCK pulses occurred less frequently in *C-GAP shRNA* embryos (Fig. 5 G). However, ROCK pulses were not decreased in *MBS shRNA* embryos that lacked discrete myosin pulses, These data suggest that ROCK pulsing is not dependent on myosin pulses. This observation, together with the fact that pulsation requires a RhoA GAP, suggests that ROCK pulses in ventral cells result from cycles of RhoA activation and inactivation (i.e., through

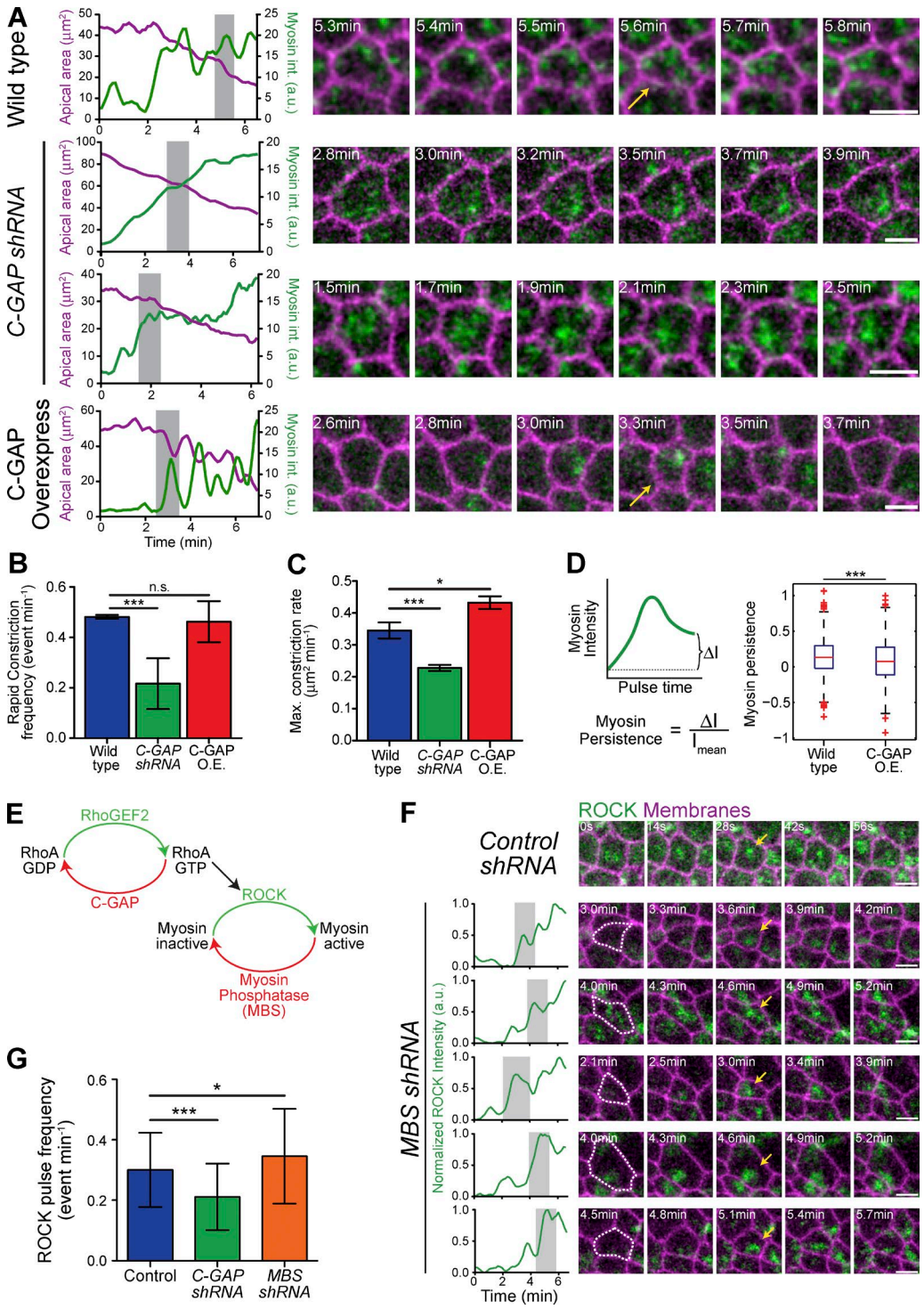

Figure 5. **C-GAP is required for normal myosin pulsing.** (A) C-GAP levels influence the amount of apical myosin that persists between pulses. Plots represent apical area and apical myosin intensity quantified for individual cells. Shaded region indicates time window used in montages on the right. Time-lapse images in montages from live embryos expressing myosin::GFP and membrane::RFP. Arrows indicate myosin pulse. (B and C) *C-GAP shRNA* disrupts contractile pulses. (B) Quantification of rapid constriction events in different genetic backgrounds. *C-GAP shRNA* has significantly lower pulse frequency (rapid constriction events per minute, 0.2164 ± 0.1 min^{-1}, two embryos, n = 123 cells) than WT (0.4815 ± 0.01 min^{-1}, two embryos, n = 181 cells) or C-GAP overexpression (O.E., 0.462 ± 0.08 min^{-1}, 2 embryos, n = 110 cells; ***, P < 0.0001; n.s., not significant). (C) Quantification of maximum constriction rate for individual cells in shows *C-GAP shRNA* has significantly lower constriction rate (0.228 ± 0.01 μm min^{-1}, three embryos, n = 190 cells) than WT (0.345 ± 0.03 μm min^{-1}, three embryos, n = 246 cells) or C-GAP OE (0.433 ± 0.02 μm min^{-1}, three embryos, n = 161 cells; ***, P < 0.0001; *, P < 0.05). Error bars represent SEM. (D) Myosin persistence measured for all WT (five embryos, 227 cells, 822 pulses) and C-GAP overexpression (three embryos, 145 cells, 447 pulses) pulses reveal significantly lower persistent myosin intensity in C-GAP overexpression embryos (***, P < 0.001; Komolgorov–Smirnov test and *t* test). Red bars represent sample medians, and boxes demarcate the 25th and 75th percentiles. (E) RhoA pathway leading to myosin activation. (F) ROCK pulsing occurs in the absence of myosin pulsing. Time-lapse images are from either *Control* or *MBS shRNA* (MBS of myosin

RhoGEF2 dynamics and C-GAP). This conclusion is also supported by the fact that RhoGEF2 can precede myosin pulses and initially appears across the entire apical cell surface. Thus, in addition to self-organization (Munjal et al., 2015), active regulation of RhoA is critical for pulsatile contractions.

C-GAP is required for the Twist-dependent transition from reversible to irreversible constrictions

Our data demonstrated that C-GAP influences pulsatile contraction within individual cells (Fig. 5, A–C), which affected how the ventral furrow folds (Videos 3–6). This led us to hypothesize that C-GAP-dependent regulation of RhoA activity at the cellular level may influence how contractility is coordinated across a tissue. Previously, we developed a computational framework that established that pulsing and shape changes of individual cells are coordinated in space and time across the ventral furrow to promote folding (Xie and Martin, 2015). Cells in WT embryos exhibit different classes of contractile pulses: ratcheted, unratcheted, or unconstricting (Xie and Martin, 2015; Fig. 6 A). Ratcheted pulses exhibit an irreversible constriction in apical area, where the constricted shape is sustained because of more persistent medioapical myosin. Unratcheted pulses resulted in an initial constriction in apical area that is then reversed (i.e., relaxes), because there is less persistent myosin to maintain the constricted state. The onset of tissue invagination is associated with a transition in cell behavior from unratcheted to ratcheted pulses (Xie and Martin, 2015). In addition to the transition in the pulse class, pulses also increase in frequency during the invagination process.

Our previous results demonstrated the transcription factor Twist is required for (a) an enrichment of ratcheted pulses, (b) pulse behavior transitioning from unratcheted to ratcheted, and (c) an increase in pulse frequency over time (Fig. 6 B; Xie and Martin, 2015). *twist* mutant and RNAi embryos fail to accumulate medioapical ROCK (Mason et al., 2013; Xie and Martin, 2015), which suggested that Twist is required for RhoGEF2-dependent activation of RhoA (Dawes-Hoang et al., 2005; Fox and Peifer, 2007; Kölsch et al., 2007). Therefore, we tested for medioapical RhoGEF2 and RhoA localization in *twist* RNAi and mutants, respectively. Twist is required for medioapical RhoGEF2 accumulation (Fig. 6 C), but not subapical, junctional RhoGEF2 (Fig. 6 D). Additionally, RhoA failed to form medioapical structures or localize to junctions in *twist* mutants and instead localized across the entire apical surface (Fig. 6 E). These results led us to hypothesize that Twist is required to increase medioapical RhoGEF2 levels over time (Fig. 2 D), thus increasing RhoA activity levels, myosin persistence, and ratcheted pulses over time (Fig. 6 B; Xie and Martin, 2015). Knowing that RhoA activation drives myosin accumulation (Fig. 1), and persistent myosin correlates with ratcheted contraction (Xie and Martin, 2015), we hypothesized that the amount of persistent myosin at the end of a pulse could be dependent on amount of RhoGEF2 relative to C-GAP. Increasing RhoA activity, by *C-GAP shRNA*, appeared to result in a more monotonic increase of myosin (Fig. 5 A), implying that RhoA activity and myosin persistence/pulse behavior are linked.

If the amount of RhoA activity after a contractile event dictates the pulse behavior (i.e., ratcheted or unratcheted), then decreasing RhoA activity should result in less persistent myosin and more unratcheted pulses. Accordingly, we have observed less persistent myosin with two unique perturbations that decrease RhoA activity: *twist* RNAi (Xie and Martin, 2015), which decreased apical RhoGEF2 levels (Fig. 6, C and D), and C-GAP OE, which decreased persistent apical myosin levels (Fig. 5, A and D). We then asked whether C-GAP OE phenocopies *twist* RNAi by quantifying (a) the amount of ratcheted contractions, (b) the transition from unratcheted to ratcheted pulses, and (c) the pulse frequency over time in C-GAP OE embryos.

C-GAP OE significantly increased the fraction of unratcheted pulses, relative to other pulse types, similar to *twist* RNAi (Fig. 6 F; Xie and Martin, 2015). Furthermore, whereas WT cells predominantly transitioned from unratcheted to ratcheted pulses at the onset of invagination, C-GAP–overexpressing embryos did not exhibit this transition, a phenotype that is similar to *twist* RNAi (Fig. 6, G and H). Pulse frequency gradually increased in WT cells during tissue invagination (from 88 s at time −200 s to 66 s at time 200 s). However, overexpressing C-GAP prevented this transition and "locks" the pulse frequency at an intermediate interval or frequency (74 s; Fig. 6 I). Interestingly, *twist* RNAi also locks pulse frequency, but at a longer interval (Xie and Martin, 2015).

Because C-GAP OE pulse behavior is similar to *twist* RNAi in that the fraction of unratcheted cell shape changes are increased, we propose that Twist is required to increase the relative levels or ratio of RhoGEF2 to C-GAP and that this ratio is a critical determinant that sets the behavior of the cell after a contractile event. Ultimately, increasing the RhoGEF2 levels over time could increase the GEF/GAP ratio, transitioning to more RhoA–ROCK–myosin activation and ratcheted pulses that promote tissue invagination.

Discussion

Our work identifies a critical role for RhoA inactivation in promoting contractility. First, expressing a CA-RhoA does not activate apical constriction but rather impedes it. Second, depleting C-GAP disrupts apical constriction, cell adhesion, and tissue folding. Because C-GAP is apically concentrated in constricting cells of the ventral furrow and loss of C-GAP does not result in obvious myosin accumulation in other cells or higher myosin levels on the basal surface, we argue that C-GAP mainly functions in the apical cortex of ventral furrow cells. We show that C-GAP is critical for the spatial organization of the RhoA pathway within the apical domain and promotes pulsatile myosin dynamics. Although previous work has demonstrated Rho GAPs are required for apical constriction in other invaginating cells or tissues (Brouns et al., 2000; Simões et al., 2006; Clay and Halloran, 2013), our work shows how a GAP is required to organize and modulate the dynamics of the contractile machinery and adherens junctions within the plane of the apical cortex for proper contractility.

phosphatase) embryos expressing GFP::ROCK and either membrane::RFP. In *MBS shRNA* embryos, ROCK increases and decreases or pulses (arrows). (G) Quantification of ROCK pulse frequency in *Control* (n = 104 cells, two embryos), *C-GAP* (n = 89 cells, two embryos), and *MBS shRNA* (n = 92 cells, two embryos) embryos shows that only loss of *C-GAP* results in fewer ROCK pulses (***, $P < 0.0001$; *, $P < 0.05$). Error bars represent SD. Bars, 5 µm.

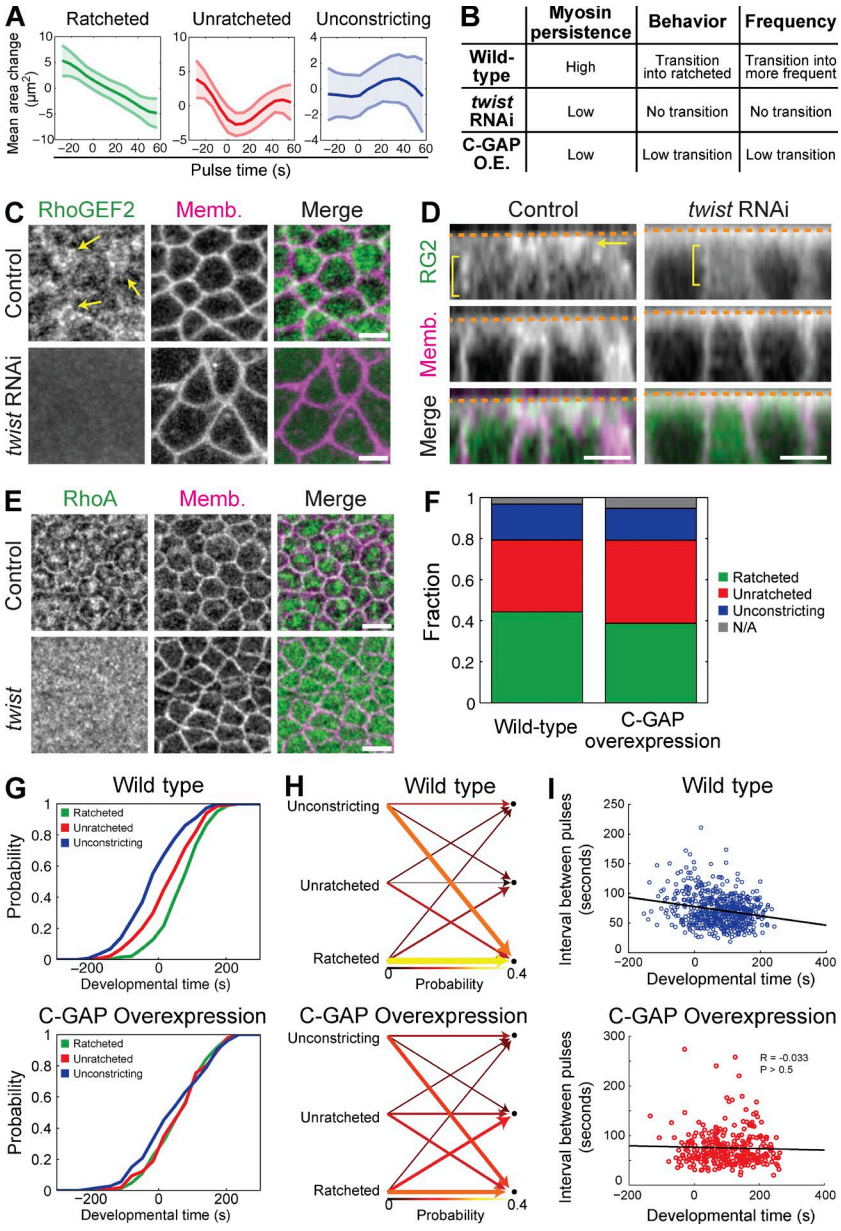

Figure 6. **Balance between RhoA activation via RhoGEF2 and inactivation via C-GAP is required for organizing pulse behavior.** (A) Mean area response within pulse behavior classes (ratcheted, unratcheted, or unconstricting) from C-GAP overexpression pulses (three embryos, 145 cells, 447 pulses). (B) Summary of pulsing phenotypes from WT, *twist* RNAi, and C-GAP OE embryos. (C and D) Live images of control (H_2O-injected) or *twist* RNAi injected embryos expressing GFP:RhoGEF2 and membrane::RFP. RhoGEF2 accumulates across the apical domain (arrows) in control embryos, which requires Twist. However, subapical/junctional RhoGEF2 (brackets) does not depend on Twist but may decrease in *twist* RNAi. (E) Images from fixed control (*twist* heterozygous) or *twist* homozygous mutant embryos, stained for RhoA and Diaphanous (subapical Dia marks membranes). RhoA is radially polarized in control embryos, but in *twist* mutants, RhoA is diffuse across the entire apical domain and lacks structure or organization. (F) Fraction of pulses from each behavior for WT and C-GAP OE embryos. C-GAP OE leads to more unratcheted pulses and fewer ratcheted pulses. (G) Probability density functions of the timing of different pulse behaviors. WT pulses transition from unconstricting and unratcheted behaviors to ratcheted behavior, whereas all pulse behaviors in C-GAP OE pulses are co-occurring. Developmental time of 0 s corresponds to beginning of tissue contraction. (H) The probability of a cell transitioning from having a pulse of a behavior class (left columns) into having a subsequent pulse of another behavior class (right columns). WT cells show biased transitions to the ratcheted state, whereas C-GAP OE cells show a much weaker transition direction. The colors and the widths of the arrows represent the probability of transition. (I) The time interval between consecutive pulses within a cell is shown with respect to developmental time. Although WT pulses become more frequent, C-GAP OE pulses occur at a constant frequency. Line shows the best fit. Bars, 5 μm.

Twist increases the GEF/GAP ratio to promote ratchet-like (sustained) contractions

Pairing a GEF and GAP for the same GTPase, which has been recently been observed in other systems (Diogon et al., 2007; Um et al., 2014), might be a conserved mechanism to promote dynamic RhoA activity required for apical constriction (Simões et al., 2006). Our data illustrates that not only are the GEF and GAP both required, but that the GEF/GAP ratio most likely changes over time to dynamically alter cell behaviors. Either lowering (*twist* RNAi or C-GAP OE) or increasing RhoA activity (*C-GAP shRNA* or CA-RhoA) "locked" cell behavior into one state and disrupted ventral furrow formation, illustrating that tuning RhoA activity throughout developmental time is essential for dynamic processes such as tissue folding (Fig. 7 and Videos 3–6). This phenomenon has been observed computationally, as modulating that concentration of GEF relative to GAP can alter the efficiency of GTPase activity cycling (Goryachev and Pokhilko, 2006).

Ventral furrow cells exhibit pulsed constriction in which cells initially exhibit reversible (i.e., unratcheted) constrictions and then exhibit constrictions where the constriction is maintained, resulting in an irreversible shape change (i.e., ratcheted). We observed that depletion of the transcription factor Twist prevents cells from transitioning from unratcheted to ratcheted constrictions, resulting in continuously unratcheted constrictions, appearing almost oscillatory (Martin et al., 2009; Xie and Martin, 2015). Understanding this result required the identification of C-GAP. In the absence of high RhoGEF2, C-GAP is present to inactivate RhoA, which could result in myosin inactivation and a drop in sustained contraction. We propose that the net increase in apical RhoGEF2, which we observe during furrow formation (Fig. 2 D), eventually outweighs C-GAP activity (Fig. 7), resulting in the observed transition from reversible (i.e., unratcheted) to irreversible (i.e., ratcheted) contractile events (Fig. 7). Consistent with this model, we have shown that overexpressing C-GAP results in a failure of cells to transition to ratcheted constrictions, suggesting that the GEF/GAP ratio sets the final outcome of a

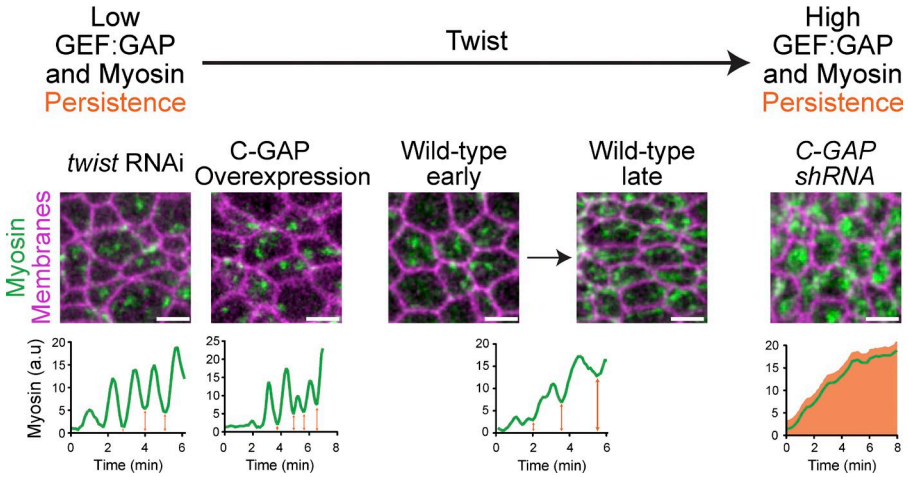

Figure 7. **The GEF/GAP ratio is a developmentally controlled mechanism to modulate cell shape.** A low RhoGEF2/C-GAP ratio, such as *twist* RNAi or C-GAP OE, results in fewer medioapical myosin fibers, less persistent myosin (orange arrows), and more unratcheted pulses. A high RhoGEF2/C-GAP ratio, as in *C-GAP shRNA*, results in "constitutive" ratcheting and less pulsing. In WT embryos, the ratio transitions, gradually increasing persistent myosin and ratchet-like contractions over time.

constriction. In addition, we have shown that myosin persistence is correlated with cells having a ratcheted constriction in both WT and C-GAP–overexpressing embryos (Xie and Martin, 2015). We have shown that *twist* RNAi embryos have significantly less tension that WT embryos, suggesting that the ratcheted or irreversible contractions generate tension that would resist expansion (Martin et al., 2010). Thus, we argue that Twist activity promotes sustained tension in cells between pulses, which is required for effective apical constriction and tissue folding.

RhoGEF2 levels increase throughout ventral furrow formation and exhibit pulsatile dynamics

We identified that RhoGEF2 (orthologue of mammalian LARG, PDZ-RhoGEF) localized with medioapical myosin structures, consistent with previous studies (Fox and Peifer, 2007; Kölsch et al., 2007). Additionally, RhoGEF2 exhibited pulsatile dynamics and RhoGEF2 pulses preceded myosin pulses, suggestive of its role in promoting or stimulating myosin pulses. This is consistent with work demonstrating that OE of RhoGEF2 promoted myosin accumulation as well as increased tension and pulse duration in *Drosophila* amnioserosa cells (Azevedo et al., 2011). However, in the amnioserosa, as well as other cells that use RhoGEF2/PDZ-RhoGEF for apical constriction (including *Drosophila* spiracle cells and mouse neural tube), it was unclear whether RhoGEF2 exhibits dynamic behavior (Simões et al., 2006; Nishimura et al., 2012). The mechanisms that promote RhoGEF2 pulsing will be an important future area of investigation. The activities of the RhoGEF2 orthologues are regulated by phosphorylation (Suzuki et al., 2003; Chikumi et al., 2004; Ying et al., 2009), and phosphorylation sites on RhoGEF2 have been identified (Zhai et al., 2008). Another potential mechanism that may influence RhoGEF2 dynamics is association with the microtubule cytoskeleton (Rogers et al., 2004; Bulgakova et al., 2013). RhoGEF2 pulses may also be mediated by its activators, such as the $G\alpha_{12/13}$ homologue *concertina* (Cta). One possibility is that Cta GTPase flux may regulate pulses of RhoGEF2 activation. LARG can function as a Gα GAP (Suzuki et al., 2003; Siehler, 2009), so it is possible that RhoGEF2 may accelerate cycling of Cta GTPase activity, and thus the RhoGEF2-Cta interaction may entrain pulsing.

C-GAP organizes both the spatial and temporal organization of the RhoA pathway

A recent study in medaka and zebrafish identified the requirement of a Rho GAP, ARHGAP18, for generation of tissue tension during gastrulation (Porazinski et al., 2015). It is unclear why a GAP, which is thought to inhibit RhoA activity, would increase tissue tension, which is typically associated with more RhoA activity. Our results and others' suggest that GAPs may be required to concentrate contractile proteins, maintain proper cell adhesion, and/or maintain robust cycling (flux) of RhoA activity (Yamada and Nelson, 2007; Miller and Bement, 2009; Ratheesh et al., 2012; Zanin et al., 2013; Breznau et al., 2015; Priya et al., 2015; Zhang and Glotzer, 2015). Clearly, there is a need for a deeper understanding for the molecular role of GAPs during morphogenesis.

Although it is clear that GEFs establish RhoA activity zones at the right place and time to organize contractility in development, less is known about how these RhoA activity and contractile zones are maintained (Bement et al., 2006). It has been hypothesized that GAPs may play a role, and our data clearly demonstrates that C-GAP is required to organize spatiotemporal RhoA pathway and contractile organization. Interestingly, recent evidence demonstrates that within RhoA zones, Rho GTPase activity cycles (or flux through the GTPase pathway) occurs (Burkel et al., 2012; Bement et al., 2015), indicating there is some mechanism for RhoA inhibition during cytoskeletal contraction. Our data suggest that C-GAP, by localizing to regions of high RhoA activity, can promote dynamic GTPase turnover where RhoA is activated. However it is unclear how C-GAP localizes to areas of high RhoA activity. C-GAP lacks obvious domains or protein–protein binding motifs, and C-GAP's closest mammalian orthologues, based on sequence homology (Hu et al., 2011), are ARHGAP20 (a RhoA-specific GAP) and TA-GAP, which have been not been thoroughly investigated (Mao et al., 2004; Yamada et al., 2005).

Our work demonstrates that although RhoA is thought to act like a switch to regulate contractility, developmental systems may use GEF:GAP modules to dial or tune RhoA activity and dynamically shift cellular behaviors according to their circumstance, purpose, or function.

Materials and methods

Fly genotypes and generation of GFP::RhoGEF2

Fly stocks and crosses used are listed in Table S2. All crosses and cages were maintained at 25°C, unless stated otherwise, and nonbalancer females and males were used to set up cages for embryo collec-

tions. To generate *Control* (*white*) and *C-GAP shRNA*, virgins of the *shRNA* line were crossed to *mat67,15* drivers with appropriate markers. Crosses were shifted to 29°C for myosin::GFP/membrane::RFP. Cages of nonbalancer siblings were maintained at 27°C for myosin::GFP/membrane::RFP, and F2 embryos were imaged. For *C-GAP* maternal germline clones, hsFLP virgins were crossed to ovoD-FRT2A males, then hsFLP;;ovoD males were crossed to virgin *RhoGAP71E/C-GAP*[*j6B9*],FRT2A mutants with GFP::ROCK and membrane::RFP markers. Larvae were heat-shocked for 2 h at 37°C on three or four consecutive days. Cages were set up with appropriate female genotypes, and mutant males and progeny were imaged. For C-GAP overexpression using *UAS>C-GAP::3xHA* (Bischof et al., 2013), *UAS>C-GAP* virgins were crossed to mat15 (for live and fixed imaging) or mat67 (for fixed imaging) males with myosin::GFP (and membrane::RFP for live imaging). Sibling, nonbalancer progeny were used to set up cages, and F2 embryos were imaged.

To generate GFP::RhoGEF2 flies, we amplified GFP-TEV-S protein pIC113 plasmid (Cheeseman and Desai, 2005). We then used standard recombineering techniques (Venken et al., 2009) and replaced the *rhoGEF2* start codon in pACMAN CH321-72J07 (obtained from BACPAC resources) with GFP::TEV::S. The resulting plasmid was confirmed via sequencing, purified, and injected in our laboratory into nanos-integrase; attp40; vk33 embryos. GFP::RhoGEF2 rescues adult fertility of trans-heterozygous mutants of several *rhogef2* alleles (*rhogef2*[1.1]/*Df(2R)ED2747*; listed in Table S2), as well as early embryonic phenotypes that are dependent on the maternal contribution of RhoGEF2, including ventral furrow formation as shown in Fig. 2 (D and E). Cellularization proceeds normally, and trans-heterozygous *rhogef2* embryos with GFP::RhoGEF2 do not have multinucleated cells typically associated with *rhogef2* mutants (Grosshans et al., 2005). The trans-heterozygous mutants with GFP::RhoGEF2 can be maintained as stable stocks.

Live and fixed imaging

For live imaging, embryos were dechorionated with 50% bleach, then washed with water and mounted, ventral side up, onto a slide coated with embryo glue (double-sided tape soaked in heptane). Spacer coverslips (1.5) were attached to glue and a coverslip was attached to create a chamber. Halocarbon 27 oil was added to chamber. Embryos were not compressed. All imaging occurred at room temperature (∼23°C).

For fixed imaging, embryos were dechorionated with bleach, then fixed in a 1:1 mix of 8% PFA in 0.1 M phosphate buffer, pH 7.4, and 100% heptane for 20–25 min and manually devitellinized or heat-fixed (HF) in boiled Triton salt solution (0.03% Triton X-100 and 0.4% NaCl in water), cooled on ice, and then devitellinized in a 1:1 heptane/methanol solution. HF embryos were then stored in 100% methanol at −20°C, and then rehydrated with PBS + 0.1% Triton X-100 (PBST). For embryo cross sections, fixed embryos were stained and then fixed again with 4% PFA in PBST for 15 min, washed with PBST, equilibrated with 50% glycerol in PBST, and manually sliced.

To visualize F-actin after PFA fixation, embryos were then incubated with Alexa Fluor 647 Phalloidin (Invitrogen) diluted in PBST overnight. Embryos were blocked with 10% BSA in PBST. For PFA-fixed embryos, Diaphanous was recognized using antibody (a gift from S. Wasserman, University of California, San Diego, La Jolla, CA) diluted at 1:5,000, E-cad (DCad-2; Developmental Studies Hybridoma Bank) at 1:50, RhoGEF2 (a gift from J. Grosshans, Georg-August-Universität Göttingen, Göttingen, Germany) at 1:1,000, HA epitope (11867423001; Roche) at 1:100–1:1,000, and Rho1 (p1D9; Developmental Studies Hybridoma Bank) at 1:50. Endogenous GFP signal was visualized for myosin::GFP. For HF embryos, Zipper (myosin heavy chain, a gift from E. Wieschaus, Princeton University, Princeton, NJ) was diluted at 1:500, Neurotactin (BP 106; Developmental Studies Hybridoma Bank) at 1:100, and HA epitope as described for PFA fixed embryos. Secondary antibodies were Alexa Fluor 488, 568, or 647 (Invitrogen), Rhodamine AffiniPure α-Mouse and Alexa Fluor 647 AffiniPure α-Rat (Jackson ImmunoResearch Laboratories, Inc.) diluted at 1:500. Primary and secondary antibodies were diluted in 5% BSA in PBST. Embryos were then mounted using AquaPolymount (Polysciences, Inc.).

For in situ hybridizations, OreR embryos were fixed with 8% formaldehyde or PFA, then devitellinized in a 1:1 heptane/methanol solution and stored in 100% methanol at −20°C. Digoxigenin-labeled probes were synthesized using plasmids described in Table S1. Embryos were transferred to 100% ethanol, washed in 100% xylenes, washed in ethanol and then methanol, then fixed in 5% formaldehyde in PBS + 0.1% Tween-20 (PBSTw). Embryos were incubated in hybridization solution (50% formamide, 5× SSC, 100 µg/ml salmon sperm DNA, 50 µg/ml heparin, and 0.1% Tween-20) at 55°C, and then incubated with 2 µl denatured probe in 100 µl hybridization solution at 55°C overnight. Embryos were washed with hybridization solution and then PBSTw, and then stained with α-digoxigenin (11093274910, diluted 1:1,000 in PBSTw; Roche) overnight at 4°C. Embryos were washed with PBSTw and then staining buffer, then a colorimetric reaction was performed using NBT/BCIP solution (11681451001; Roche), and quenching was performed with PBSTw and ethanol washes. Embryos were rinsed with xylenes, mounted with Permount (Thermo Fisher Scientific) or Aqua-Polymount, and imaged using an Eclipse Ti-S Microscope (Nikon), 10×/0.25NA objective (Nikon), Spot Idea camera, and Spot Software (SPOT Imaging). Reagents for the GAP in situ screen were provided by V. Hatini (Tufts University, Boston, MA).

Unless otherwise stated, all fluorescent images were acquired on a confocal microscope (LSM 710; ZEISS) with a 40×/1.2 Apochromat water objective (ZEISS), an argon ion, 561-nm diode, 594-nm HeNe, and 633-nm HeNe lasers, and Zen Software. Pinhole settings ranged from 1–3 airy units (1 airy units for fixed imaging and ∼1.5–3 airy units for live imaging). Because it expressed at such low levels, imaging for GFP::RhoGEF2 required 3 airy units and a much slower scan speed. For improved visualization of GFP::RhoGEF2 in Video 2, exponential bleach correction was applied using FIJI; however, no such processing was used for images shown in Fig. 2 (D–F) or Fig. S2. For two-color, live imaging, simultaneous excitation was used with bandpass filters set at ∼499–561 nm for GFP and ∼599–696 nm for ChFP. For imaging apical myosin (Sqh::mCherry) meshwork with GFP::RhoGEF2 (Fig. 2 C), Applied Precision DeltaVision Ultimate Focus Inverted Olympus X71 microscope with total internal reflection fluorescence microscope module, 488- and 568-nm lasers, 100× total internal reflection fluorescence microscope objective, and 470-nm/525-nm (GFP) and 575-nm/630-nm (mCherry) excitation/emission filter sets was used.

Drug and RNA injections

C3 exoenzyme protein (CT03; Cytoskeleton, Inc.) was resuspended at 1 mg/ml, dialyzed into PBS, and stored at −80°C. PBS was injected as control buffer. To synthesize capped mRNA for RhoA-WT and CA from plasmids previously described (Simões et al., 2014) and for C-GAP and C-GAP mutants, we used mMESSAGE mMACHINE SP6 Transcription kit (Ambion) and injected embryos with mRNA at 0.5–1 µg/µl. To synthesize double-stranded RNA for *twist* RNAi using methods and primers previously described (Martin et al., 2010), we used MEGAscript T7 Transcription kit (Ambion).

Dechorionated embryos were mounted ventral side up for furrow injection then desiccated for 4–10 min using Drierite (Drierite Company). A 1:1 mixture of halocarbon 700:halocarbon 27 oils was added over the embryo for injection. Embryos were injected laterally

during mid-to-late cellularization (furrow canals at base of nuclei; Fig. 1, A and B) or during ventral furrow formation (furrow canals at yolk, cephalic furrow ingressing; Fig. S1) for C3 injections and imaged immediately after injection (∼3–5 min after injection). For injection of capped RNA of CA-RhoA and WT-RhoA (Simões et al., 2014), embryos were injected laterally at one pole at the end of yolk clearing and the initiation of cellularization, roughly 1 h before imaging (Fig. 1 C and Video 1). For injection of capped RNA of C-GAP RNA (Fig. 3, F and G), embryos were injection around the initiation of pole formation and imaged ∼1.5–2 h after injection. After injection, injection oil was removed and embryos were mounted as described for live imaging and incubated at room temperature or 25°C. For *twist* RNAi experiments (Fig. 6, D and E), embryos were injected with *twist* dsRNA (Martin et al., 2010) or water (control) immediately after egg laying, before pole cell formation, and incubated at room temperature or 25°C for 2.5–3 h before imaging.

Image processing and analysis

Images were processed using MATLAB (MathWorks), FIJI, and Photoshop (Adobe Systems, Inc.). A Gaussian filter (kernel = 1 pixel) was applied to images. Apical images are maximum intensity projections of multiple z-sections (∼2–5 µm). Subapical images are ∼1–2 µm below the apical sections.

Image segmentation for temporal quantification of area and myosin intensities was performed using custom MATLAB software titled EDGE (Embryo Development Geometry Explorer; Gelbart et al., 2012). Raw images were subjected to Gaussian filter (1 pixel) processed via background subtraction to remove cytoplasmic myosin::ChFP or myosin::GFP by subtracting cytoplasmic intensity values two SDs from the mean. We made maximum intensity projections, imported mages were imported into EDGE, and cell membranes were automatically detected and manually corrected. Cell area and integrated fluorescence intensity of myosin were quantified (Figs. 1, 5, and 6).

To compare the frequency of instances of rapid area reduction between embryos (Fig. 5 B), we used methods previously described (Vasquez et al., 2014). In brief, we smoothed apical area curves and calculated instantaneous rates for each time point. Rapid area reductions were defined as instances where the constriction rate exceeded a threshold of one SD above the mean rate for all WT cells. To compare maximum constriction rates among WT, *C-GAP shRNA*, and C-GAP OE (Fig. 5 C), we identified the instance of the maximum constriction rate of each cell. The identified maximum constriction rates were for all cells of each condition. To compare ROCK pulsing frequency, we computationally and manually identified ROCK pulses using methods previously described (Mason et al., 2013).

Linescans of myosin::GFP in *control* (*white*) and *C-GAP shRNA* cells were generated using FIJI (Fig. 4 B). At least 20 cells were analyzed for each genotype. Ratios of medioapical to junctional myosin in CA-RhoA (Fig. 1 E) were obtained using FIJI, by manually drawing a line around cell junctions to determine mean intensity. Circles or ellipses were drawn over medioapical region to obtain mean intensity. For each cell, medioapical intensities were divided by junctional intensity and then averaged across all cells. For RhoGEF2 and myosin pulse analysis (Fig. 2 G), FIJI MTrackJ plug-in was used to manually identify local peaks/pulses of GFP::RhoGEF2 and myosin::RFP from five embryos and 187 pulses and time delay were plotted using Prism (box and whiskers, 5th and 95th percentile).

Statistical analyses were performed in Prism (GraphPad; Figs. 1 and 5) and MATLAB (Fig. 6). Datasets were subjected to Komolgorov–Smirnov tests to determine distributions and used unpaired, two-tailed, *t* test for pulse behavior (Figs. 1, 5, and 6). All error bars are listed in figure legends, and results of tests are represented as p-values.

Quantification of C-GAP OE

To quantify degree of C-GAP OE in mat15>C-GAP embryos used for live imaging and pulse analyses, we collected 100 stage 5 and 6 embryos from four genotypes: Oregon R (WT), *mat15>GAL4*, *UAS>C-GAP*, and *mat15>C-GAP* (C-GAP OE). RNA was extracted from pooled embryos using TRIzol (Thermo Fisher Scientific) and the manufacturer's protocol. Precipitated RNA was resuspended in water, Dnase I treated (New England Biolabs, Inc.), and concentration quantified. Superscript III One-Step RT-PCR System (Invitrogen) was used to perform reverse transcription reaction and PCR, following the manufacturer's protocol, with minor exceptions. 250 ng RNA was added to reaction, and 25 PCR amplification cycles were used. Gene-specific primers for RpL32, a ribosomal protein as a control, were manually designed, and two unique C-GAP primer sets were designed using Universal ProbeLibrary Assay Design Center (Roche) and FlyPrimerBank (Hu et al., 2013). Products were run on an agarose gel and visualized using ethidium bromide and Bio-Rad ChemiDoc MP. Quantifications were performed using FIJI gel analyzer plug-in. C-GAP OE is ∼1.5 times higher than endogenous gene expression (Fig. S4 C).

Pulse quantification and classification

Pulse quantification used a previously published framework, where Gaussian models were fitted to the myosin intensity signal and used to extract local changes in apical area (Xie and Martin, 2015). Determination of area behaviors during pulses in three C-GAP OE embryos (145 cells and 447 pulses) were done by coclustering them with area response data of pulses from five WT embryos (227 cells and 822 pulses) and five *twist* RNAi embryos used in the previous study.

Online supplemental material

Fig. S1 shows that RhoA activity is required to maintain apical Myosin. Fig. S2 shows that GFP::RhoGEF2 forms structures across the apical surface, localizes subapically to junctions, and is planar polarized in the lateral (germband) cells. Fig. S3 shows that C-GAP is required for cellularization, which precedes ventral furrow formation. Fig. S4 shows that C-GAP shRNA embryos phenotypes appear to be ventral specific. Video 1 shows that CA RhoA OE alters myosin dynamics and apical constriction during ventral furrow formation. Video 2 shows RhoGEF2 and myosin pulsatile dynamics during ventral furrow formation. Video 3 shows WT ventral furrow formation. Video 4 shows a C-GAP shRNA embryo with mild ventral furrow phenotype. Video 5 shows a C-GAP shRNA embryo with severe ventral furrow phenotype. Video 6 shows a C-GAP overexpression embryo. Table S1 describes Rho-family GAP expression and screen during early embryogenesis. Table S2 lists genotypes for fly stocks used in this study. Online supplemental material is available at http://www.jcb.org/cgi/content/full/jcb.201603077/DC1.

Acknowledgments

We would like to thank members of the Martin Lab for discussions and advice. We would also like to thank Victor Hatini, Jennifer Zallen (Memorial Sloan-Kettering Cancer Center), Sérgio Simões (University of Toronto), Yohanns Bellaïche (Institut Curie), Jörg Grosshans, Susan Parkhurst (Fred Hutchinson Research Cancer Center), Eric Wieschaus, the Zurich ORFeome Project (University of Zurich), P[acman] library project (National Institutes of Health and Howard Hughes Medial Institute), Hugo Bellen (Baylor College of Medicine), Roger Hoskins (Lawrence Berkeley National Laboratory), BACPAC Resources Center at Children's Hospital Oakland Research Institute, and TRiP at Harvard Medical School (National Institutes of Health/National Institute of General Medical Sciences R01-GM084947) for constructs, trans-

genic flies, and antibodies. We also thank Eliza Vasile at the Swanson Biotechnology Center at the Koch Institute for Integrative Cancer Research at the Massachusetts Institute of Technology for imaging expertise.

This work was supported by a grant from the American Cancer Society (125792-RSG-14-039-01-CSM) to A.C. Martin.

The authors declare no competing financial interests.

Submitted: 22 March 2016
Accepted: 15 July 2016

References

Azevedo, D., M. Antunes, S. Prag, X. Ma, U. Häcker, G.W. Brodland, M.S. Hutson, J. Solon, and A. Jacinto. 2011. DRhoGEF2 regulates cellular tension and cell pulsations in the Amnioserosa during *Drosophila* dorsal closure. *PLoS One.* 6:e23964. http://dx.doi.org/10.1371/journal.pone.0023964

Bakal, C., J. Aach, G. Church, and N. Perrimon. 2007. Quantitative morphological signatures define local signaling networks regulating cell morphology. *Science.* 316:1753–1756. http://dx.doi.org/10.1126/science.1140324

Barrett, K., M. Leptin, and J. Settleman. 1997. The Rho GTPase and a putative RhoGEF mediate a signaling pathway for the cell shape changes in *Drosophila* gastrulation. *Cell.* 91:905–915. http://dx.doi.org/10.1016/S0092-8674(00)80482-1

Bement, W.M., A.L. Miller, and G. von Dassow. 2006. Rho GTPase activity zones and transient contractile arrays. *BioEssays.* 28:983–993. http://dx.doi.org/10.1002/bies.20477

Bement, W.M., M. Leda, A.M. Moe, A.M. Kita, M.E. Larson, A.E. Golding, C. Pfeuti, K.-C. Su, A.L. Miller, A.B. Goryachev, and G. von Dassow. 2015. Activator-inhibitor coupling between Rho signalling and actin assembly makes the cell cortex an excitable medium. *Nat. Cell Biol.* 17:1471–1483. http://dx.doi.org/10.1038/ncb3251

Bischof, J., M. Björklund, E. Furger, C. Schertel, J. Taipale, and K. Basler. 2013. A versatile platform for creating a comprehensive UAS-ORFeome library in *Drosophila*. *Development.* 140:2434–2442. http://dx.doi.org/10.1242/dev.088757

Blanchard, G.B., S. Murugesu, R.J. Adams, A. Martinez-Arias, and N. Gorfinkiel. 2010. Cytoskeletal dynamics and supracellular organisation of cell shape fluctuations during dorsal closure. *Development.* 137:2743–2752. http://dx.doi.org/10.1242/dev.045872

Bos, J.L., H. Rehmann, and A. Wittinghofer. 2007. GEFs and GAPs: critical elements in the control of small G proteins. *Cell.* 129:865–877. http://dx.doi.org/10.1016/j.cell.2007.05.018

Breznau, E.B., A.C. Semack, T. Higashi, and A.L. Miller. 2015. MgcRacGAP restricts active RhoA at the cytokinetic furrow and both RhoA and Rac1 at cell-cell junctions in epithelial cells. *Mol. Biol. Cell.* 26:2439–2455. http://dx.doi.org/10.1091/mbc.E14-11-1553

Brouns, M.R., S.F. Matheson, K.Q. Hu, I. Delalle, V.S. Caviness, J. Silver, R.T. Bronson, and J. Settleman. 2000. The adhesion signaling molecule p190 RhoGAP is required for morphogenetic processes in neural development. *Development.* 127:4891–4903.

Bulgakova, N.A., I. Grigoriev, A.S. Yap, A. Akhmanova, and N.H. Brown. 2013. Dynamic microtubules produce an asymmetric E-cadherin-Bazooka complex to maintain segment boundaries. *J. Cell Biol.* 201:887–901. http://dx.doi.org/10.1083/jcb.201211159

Burkel, B.M., H.A. Benink, E.M. Vaughan, G. von Dassow, and W.M. Bement. 2012. A Rho GTPase signal treadmill backs a contractile array. *Dev. Cell.* 23:384–396. http://dx.doi.org/10.1016/j.devcel.2012.05.025

Burridge, K., and E.S. Wittchen. 2013. The tension mounts: stress fibers as force-generating mechanotransducers. *J. Cell Biol.* 200:9–19. http://dx.doi.org/10.1083/jcb.201210090

Cheeseman, I.M., and A. Desai. 2005. A combined approach for the localization and tandem affinity purification of protein complexes from metazoans. *Sci. STKE.* 2005:pl1. http://dx.doi.org/10.1126/stke.2662005pl1

Chikumi, H., A. Barac, B. Behbahani, Y. Gao, H. Teramoto, Y. Zheng, and J.S. Gutkind. 2004. Homo- and hetero-oligomerization of PDZ-RhoGEF, LARG and p115RhoGEF by their C-terminal region regulates their in vivo Rho GEF activity and transforming potential. *Oncogene.* 23:233–240. http://dx.doi.org/10.1038/sj.onc.1207012

Chou, T.B., and N. Perrimon. 1992. Use of a yeast site-specific recombinase to produce female germline chimeras in *Drosophila*. *Genetics.* 131:643–653.

Clay, M.R., and M.C. Halloran. 2013. Rho activation is apically restricted by Arhgap1 in neural crest cells and drives epithelial-to-mesenchymal transition. *Development.* 140:3198–3209. http://dx.doi.org/10.1242/dev.095448

Costa, M., E.T. Wilson, and E. Wieschaus. 1994. A putative cell signal encoded by the folded gastrulation gene coordinates cell shape changes during *Drosophila* gastrulation. *Cell.* 76:1075–1089. http://dx.doi.org/10.1016/0092-8674(94)90384-0

Crawford, J.M., N. Harden, T. Leung, L. Lim, and D.P. Kiehart. 1998. Cellularization in *Drosophila melanogaster* is disrupted by the inhibition of rho activity and the activation of Cdc42 function. *Dev. Biol.* 204:151–164. http://dx.doi.org/10.1006/dbio.1998.9061

Dawes-Hoang, R.E., K.M. Parmar, A.E. Christiansen, C.B. Phelps, A.H. Brand, and E.F. Wieschaus. 2005. folded gastrulation, cell shape change and the control of myosin localization. *Development.* 132:4165–4178. http://dx.doi.org/10.1242/dev.01938

Diogon, M., F. Wissler, S. Quintin, Y. Nagamatsu, S. Sookhareea, F. Landmann, H. Hutter, N. Vitale, and M. Labouesse. 2007. The RhoGAP RGA-2 and LET-502/ROCK achieve a balance of actomyosin-dependent forces in *C. elegans* epidermis to control morphogenesis. *Development.* 134:2469–2479. http://dx.doi.org/10.1242/dev.005074

Fox, D.T., and M. Peifer. 2007. Abelson kinase (Abl) and RhoGEF2 regulate actin organization during cell constriction in *Drosophila*. *Development.* 134:567–578. http://dx.doi.org/10.1242/dev.02748

Gelbart, M.A., B. He, A.C. Martin, S.Y. Thiberge, E.F. Wieschaus, and M. Kaschube. 2012. Volume conservation principle involved in cell lengthening and nucleus movement during tissue morphogenesis. *Proc. Natl. Acad. Sci. USA.* 109:19298–19303. http://dx.doi.org/10.1073/pnas.1205258109

Goryachev, A.B., and A.V. Pokhilko. 2006. Computational model explains high activity and rapid cycling of Rho GTPases within protein complexes. *PLOS Comput. Biol.* 2:e172. (published erratum appears in *PLOS Comput. Biol.* 2007. 3:e136) http://dx.doi.org/10.1371/journal.pcbi.0020172

Greenberg, L., and V. Hatini. 2011. Systematic expression and loss-of-function analysis defines spatially restricted requirements for *Drosophila* RhoGEFs and RhoGAPs in leg morphogenesis. *Mech. Dev.* 128:5–17. http://dx.doi.org/10.1016/j.mod.2010.09.001

Grosshans, J., C. Wenzl, H.-M. Herz, S. Bartoszewski, F. Schnorrer, N. Vogt, H. Schwarz, and H.-A. Müller. 2005. RhoGEF2 and the formin Dia control the formation of the furrow canal by directed actin assembly during *Drosophila* cellularisation. *Development.* 132:1009–1020. http://dx.doi.org/10.1242/dev.01669

Häcker, U., and N. Perrimon. 1998. DRhoGEF2 encodes a member of the Dbl family of oncogenes and controls cell shape changes during gastrulation in *Drosophila*. *Genes Dev.* 12:274–284. http://dx.doi.org/10.1101/gad.12.2.274

He, L., X. Wang, H.L. Tang, and D.J. Montell. 2010. Tissue elongation requires oscillating contractions of a basal actomyosin network. *Nat. Cell Biol.* 12:1133–1142. http://dx.doi.org/10.1038/ncb2124

Hu, Y., I. Flockhart, A. Vinayagam, C. Bergwitz, B. Berger, N. Perrimon, and S.E. Mohr. 2011. An integrative approach to ortholog prediction for disease-focused and other functional studies. *BMC Bioinformatics.* 12:357. http://dx.doi.org/10.1186/1471-2105-12-357

Hu, Y., R. Sopko, M. Foos, C. Kelley, I. Flockhart, N. Ammeux, X. Wang, L. Perkins, N. Perrimon, and S.E. Mohr. 2013. FlyPrimerBank: an online database for *Drosophila melanogaster* gene expression analysis and knockdown evaluation of RNAi reagents. *G3 (Bethesda).* 3:1607–1616. http://dx.doi.org/10.1534/g3.113.007021

Jaffe, A.B., and A. Hall. 2005. Rho GTPases: biochemistry and biology. *Annu. Rev. Cell Dev. Biol.* 21:247–269. http://dx.doi.org/10.1146/annurev.cellbio.21.020604.150721

Jodoin, J.N., J.S. Coravos, S. Chanet, C.G. Vasquez, M. Tworoger, E.R. Kingston, L.A. Perkins, N. Perrimon, and A.C. Martin. 2015. Stable force balance between epithelial cells arises from F-actin turnover. *Dev. Cell.* 35:685–697. http://dx.doi.org/10.1016/j.devcel.2015.11.018

Kasza, K.E., D.L. Farrell, and J.A. Zallen. 2014. Spatiotemporal control of epithelial remodeling by regulated myosin phosphorylation. *Proc. Natl. Acad. Sci. USA.* 111:11732–11737. http://dx.doi.org/10.1073/pnas.1400520111

Kerridge, S., A. Munjal, J.-M. Philippe, A. Jha, A.G. de las Bayonas, A.J. Saurin, and T. Lecuit. 2016. Modular activation of Rho1 by GPCR signalling imparts polarized myosin II activation during morphogenesis. *Nat. Cell Biol.* 18:261–270. http://dx.doi.org/10.1038/ncb3302

Kölsch, V., T. Seher, G.J. Fernandez-Ballester, L. Serrano, and M. Leptin. 2007. Control of *Drosophila* gastrulation by apical localization of adherens

junctions and RhoGEF2. *Science.* 315:384–386. http://dx.doi.org/10.1126/science.1134833

Krugmann, S., K.E. Anderson, S.H. Ridley, N. Risso, A. McGregor, J. Coadwell, K. Davidson, A. Eguinoa, C.D. Ellson, P. Lipp, et al. 2002. Identification of ARAP3, a novel PI3K effector regulating both Arf and Rho GTPases, by selective capture on phosphoinositide affinity matrices. *Mol. Cell.* 9:95–108. http://dx.doi.org/10.1016/S1097-2765(02)00434-3

Leptin, M. 1991. twist and snail as positive and negative regulators during *Drosophila* mesoderm development. *Genes Dev.* 5:1568–1576. http://dx.doi.org/10.1101/gad.5.9.1568

Levayer, R., A. Pelissier-Monier, and T. Lecuit. 2011. Spatial regulation of Dia and Myosin-II by RhoGEF2 controls initiation of E-cadherin endocytosis during epithelial morphogenesis. *Nat. Cell Biol.* 13:529–540. http://dx.doi.org/10.1038/ncb2224

Magie, C.R., M.R. Meyer, M.S. Gorsuch, and S.M. Parkhurst. 1999. Mutations in the Rho1 small GTPase disrupt morphogenesis and segmentation during early *Drosophila* development. *Development.* 126:5353–5364.

Manning, A.J., K.A. Peters, M. Peifer, and S.L. Rogers. 2013. Regulation of epithelial morphogenesis by the G protein-coupled receptor mist and its ligand fog. *Sci. Signal.* 6:ra98. http://dx.doi.org/10.1126/scisignal.2004427

Mao, M., M.C. Biery, S.V. Kobayashi, T. Ward, G. Schimmack, J. Burchard, J.M. Schelter, H. Dai, Y.D. He, and P.S. Linsley. 2004. T lymphocyte activation gene identification by coregulated expression on DNA microarrays. *Genomics.* 83:989–999. http://dx.doi.org/10.1016/j.ygeno.2003.12.019

Martin, A.C., and B. Goldstein. 2014. Apical constriction: themes and variations on a cellular mechanism driving morphogenesis. *Development.* 141:1987–1998. http://dx.doi.org/10.1242/dev.102228

Martin, A.C., M. Kaschube, and E.F. Wieschaus. 2009. Pulsed contractions of an actin-myosin network drive apical constriction. *Nature.* 457:495–499. http://dx.doi.org/10.1038/nature07522

Martin, A.C., M. Gelbart, R. Fernandez-Gonzalez, M. Kaschube, and E.F. Wieschaus. 2010. Integration of contractile forces during tissue invagination. *J. Cell Biol.* 188:735–749. http://dx.doi.org/10.1083/jcb.200910099

Mason, F.M., M. Tworoger, and A.C. Martin. 2013. Apical domain polarization localizes actin-myosin activity to drive ratchet-like apical constriction. *Nat. Cell Biol.* 15:926–936. http://dx.doi.org/10.1038/ncb2796

Miller, A.L., and W.M. Bement. 2009. Regulation of cytokinesis by Rho GTPase flux. *Nat. Cell Biol.* 11:71–77. http://dx.doi.org/10.1038/ncb1814

Miura, K., K.M. Jacques, S. Stauffer, A. Kubosaki, K. Zhu, D.S. Hirsch, J. Resau, Y. Zheng, and P.A. Randazzo. 2002. ARAP1: a point of convergence for Arf and Rho signaling. *Mol. Cell.* 9:109–119. http://dx.doi.org/10.1016/S1097-2765(02)00428-8

Munjal, A., J.-M. Philippe, E. Munro, and T. Lecuit. 2015. A self-organized biomechanical network drives shape changes during tissue morphogenesis. *Nature.* 524:351–355. http://dx.doi.org/10.1038/nature14603

Munro, E., J. Nance, and J.R. Priess. 2004. Cortical flows powered by asymmetrical contraction transport PAR proteins to establish and maintain anterior-posterior polarity in the early *C. elegans* embryo. *Dev. Cell.* 7:413–424. http://dx.doi.org/10.1016/j.devcel.2004.08.001

Nakaya, Y., E.W. Sukowati, Y. Wu, and G. Sheng. 2008. RhoA and microtubule dynamics control cell-basement membrane interaction in EMT during gastrulation. *Nat. Cell Biol.* 10:765–775. http://dx.doi.org/10.1038/ncb1739

Nishimura, T., H. Honda, and M. Takeichi. 2012. Planar cell polarity links axes of spatial dynamics in neural-tube closure. *Cell.* 149:1084–1097. http://dx.doi.org/10.1016/j.cell.2012.04.021

Perkins, L.A., L. Holderbaum, R. Tao, Y. Hu, R. Sopko, K. McCall, D. Yang-Zhou, I. Flockhart, R. Binari, H.-S. Shim, et al. 2015. The Transgenic RNAi Project at Harvard Medical School: resources and validation. *Genetics.* 201:843–852. http://dx.doi.org/10.1534/genetics.115.180208

Piekny, A.J., and M. Glotzer. 2008. Anillin is a scaffold protein that links RhoA, actin, and myosin during cytokinesis. *Curr. Biol.* 18:30–36. http://dx.doi.org/10.1016/j.cub.2007.11.068

Polyakov, O., B. He, M. Swan, J.W. Shaevitz, M. Kaschube, and E. Wieschaus. 2014. Passive mechanical forces control cell-shape change during *Drosophila* ventral furrow formation. *Biophys. J.* 107:998–1010. http://dx.doi.org/10.1016/j.bpj.2014.07.013

Porazinski, S., H. Wang, Y. Asaoka, M. Behrndt, T. Miyamoto, H. Morita, S. Hata, T. Sasaki, S.F.G. Krens, Y. Osada, et al. 2015. YAP is essential for tissue tension to ensure vertebrate 3D body shape. *Nature.* 521:217–221. http://dx.doi.org/10.1038/nature14215

Priya, R., G.A. Gomez, S. Budnar, S. Verma, H.L. Cox, N.A. Hamilton, and A.S. Yap. 2015. Feedback regulation through myosin II confers robustness on RhoA signalling at E-cadherin junctions. *Nat. Cell Biol.* 17:1282–1293. http://dx.doi.org/10.1038/ncb3239

Ratheesh, A., G.A. Gomez, R. Priya, S. Verma, E.M. Kovacs, K. Jiang, N.H. Brown, A. Akhmanova, S.J. Stehbens, and A.S. Yap. 2012. Centralspindlin and α-catenin regulate Rho signalling at the epithelial zonula adherens. *Nat. Cell Biol.* 14:818–828. http://dx.doi.org/10.1038/ncb2532

Rauzi, M., P.-F. Lenne, and T. Lecuit. 2010. Planar polarized actomyosin contractile flows control epithelial junction remodelling. *Nature.* 468:1110–1114. http://dx.doi.org/10.1038/nature09566

Rauzi, M., U. Krzic, T.E. Saunders, M. Krajnc, P. Ziherl, L. Hufnagel, and M. Leptin. 2015. Embryo-scale tissue mechanics during *Drosophila* gastrulation movements. *Nat. Commun.* 6:8677. http://dx.doi.org/10.1038/ncomms9677

Ridley, A.J., and A. Hall. 1992. The small GTP-binding protein rho regulates the assembly of focal adhesions and actin stress fibers in response to growth factors. *Cell.* 70:389–399. http://dx.doi.org/10.1016/0092-8674(92)90163-7

Ridley, A.J., A.J. Self, F. Kasmi, H.F. Paterson, A. Hall, C.J. Marshall, and C. Ellis. 1993. rho family GTPase activating proteins p190, bcr and rhoGAP show distinct specificities in vitro and in vivo. *EMBO J.* 12:5151–5160.

Rogers, S.L., U. Wiedemann, U. Häcker, C. Turck, and R.D. Vale. 2004. *Drosophila* RhoGEF2 associates with microtubule plus ends in an EB1-dependent manner. *Curr. Biol.* 14:1827–1833. http://dx.doi.org/10.1016/j.cub.2004.09.078

Sailem, H., V. Bousgouni, S. Cooper, and C. Bakal. 2014. Cross-talk between Rho and Rac GTPases drives deterministic exploration of cellular shape space and morphological heterogeneity. *Open Biol.* 4:130132. http://dx.doi.org/10.1098/rsob.130132

Salbreux, G., G. Charras, and E. Paluch. 2012. Actin cortex mechanics and cellular morphogenesis. *Trends Cell Biol.* 22:536–545. http://dx.doi.org/10.1016/j.tcb.2012.07.001

Sawyer, J.M., J.R. Harrell, G. Shemer, J. Sullivan-Brown, M. Roh-Johnson, and B. Goldstein. 2010. Apical constriction: a cell shape change that can drive morphogenesis. *Dev. Biol.* 341:5–19. http://dx.doi.org/10.1016/j.ydbio.2009.09.009

Schumacher, S., T. Gryzik, S. Tannebaum, and H.-A.J. Müller. 2004. The RhoGEF Pebble is required for cell shape changes during cell migration triggered by the *Drosophila* FGF receptor Heartless. *Development.* 131:2631–2640. http://dx.doi.org/10.1242/dev.01149

Siehler, S. 2009. Regulation of RhoGEF proteins by G12/13-coupled receptors. *Br. J. Pharmacol.* 158:41–49. http://dx.doi.org/10.1111/j.1476-5381.2009.00121.x

Simões, S., B. Denholm, D. Azevedo, S. Sotillos, P. Martin, H. Skaer, J.C.G. Hombría, and A. Jacinto. 2006. Compartmentalisation of Rho regulators directs cell invagination during tissue morphogenesis. *Development.* 133:4257–4267. http://dx.doi.org/10.1242/dev.02588

Simões, S. de M., A. Mainieri, and J.A. Zallen. 2014. Rho GTPase and Shroom direct planar polarized actomyosin contractility during convergent extension. *J. Cell Biol.* 204:575–589. http://dx.doi.org/10.1083/jcb.201307070

Smallhorn, M., M.J. Murray, and R. Saint. 2004. The epithelial-mesenchymal transition of the *Drosophila* mesoderm requires the Rho GTP exchange factor Pebble. *Development.* 131:2641–2651. http://dx.doi.org/10.1242/dev.01150

Suzuki, N., S. Nakamura, H. Mano, and T. Kozasa. 2003. Galpha 12 activates Rho GTPase through tyrosine-phosphorylated leukemia-associated RhoGEF. *Proc. Natl. Acad. Sci. USA.* 100:733–738. http://dx.doi.org/10.1073/pnas.0234057100

Tojkander, S., G. Gateva, and P. Lappalainen. 2012. Actin stress fibers—assembly, dynamics and biological roles. *J. Cell Sci.* 125:1855–1864. http://dx.doi.org/10.1242/jcs.098087

Um, K., S. Niu, J.G. Duman, J.X. Cheng, Y.-K. Tu, B. Schwechter, F. Liu, L. Hiles, A.S. Narayanan, R.T. Ash, et al. 2014. Dynamic control of excitatory synapse development by a Rac1 GEF/GAP regulatory complex. *Dev. Cell.* 29:701–715. http://dx.doi.org/10.1016/j.devcel.2014.05.011

Vasquez, C.G., and A.C. Martin. 2016. Force transmission in epithelial tissues. *Dev. Dyn.* 245:361–371. http://dx.doi.org/10.1002/dvdy.24384

Vasquez, C.G., M. Tworoger, and A.C. Martin. 2014. Dynamic myosin phosphorylation regulates contractile pulses and tissue integrity during epithelial morphogenesis. *J. Cell Biol.* 206:435–450. http://dx.doi.org/10.1083/jcb.201402004

Venken, K.J.T., J.W. Carlson, K.L. Schulze, H. Pan, Y. He, R. Spokony, K.H. Wan, M. Koriabine, P.J. de Jong, K.P. White, et al. 2009. Versatile P[acman]

BAC libraries for transgenesis studies in *Drosophila melanogaster*. *Nat. Methods.* 6:431–434. http://dx.doi.org/10.1038/nmeth.1331

Vincent, S., and J. Settleman. 1999. Inhibition of RhoGAP activity is sufficient for the induction of Rho-mediated actin reorganization. *Eur. J. Cell Biol.* 78:539–548. http://dx.doi.org/10.1016/S0171-9335(99)80019-3

Weng, M., and E. Wieschaus. 2016. Myosin-dependent remodeling of adherens junctions protects junctions from Snail-dependent disassembly. *J. Cell Biol.* 212:219–229. http://dx.doi.org/10.1083/jcb.201508056

Wennerberg, K., M.-A. Forget, S.M. Ellerbroek, W.T. Arthur, K. Burridge, J. Settleman, C.J. Der, and S.H. Hansen. 2003. Rnd proteins function as RhoA antagonists by activating p190 RhoGAP. *Curr. Biol.* 13:1106–1115. http://dx.doi.org/10.1016/S0960-9822(03)00418-4

Xie, S., and A.C. Martin. 2015. Intracellular signalling and intercellular coupling coordinate heterogeneous contractile events to facilitate tissue folding. *Nat. Commun.* 6:7161. http://dx.doi.org/10.1038/ncomms8161

Yamada, S., and W.J. Nelson. 2007. Localized zones of Rho and Rac activities drive initiation and expansion of epithelial cell-cell adhesion. *J. Cell Biol.* 178:517–527. http://dx.doi.org/10.1083/jcb.200701058

Yamada, T., T. Sakisaka, S. Hisata, T. Baba, and Y. Takai. 2005. RA-RhoGAP, Rap-activated Rho GTPase-activating protein implicated in neurite outgrowth through Rho. *J. Biol. Chem.* 280:33026–33034. http://dx.doi.org/10.1074/jbc.M504587200

Yeung, C.-Y.C., S.H. Taylor, R. Garva, D.F. Holmes, L.A. Zeef, R. Soininen, R.P. Boot-Handford, and K.E. Kadler. 2014. Arhgap28 is a RhoGAP that inactivates RhoA and downregulates stress fibers. *PLoS One.* 9:e107036. http://dx.doi.org/10.1371/journal.pone.0107036

Ying, Z., F.R.C. Giachini, R.C. Tostes, and R.C. Webb. 2009. PYK2/PDZ-RhoGEF links Ca2+ signaling to RhoA. *Arterioscler. Thromb. Vasc. Biol.* 29:1657–1663. http://dx.doi.org/10.1161/ATVBAHA.109.190892

Zanin, E., A. Desai, I. Poser, Y. Toyoda, C. Andree, C. Moebius, M. Bickle, B. Conradt, A. Piekny, and K. Oegema. 2013. A conserved RhoGAP limits M phase contractility and coordinates with microtubule asters to confine RhoA during cytokinesis. *Dev. Cell.* 26:496–510. http://dx.doi.org/10.1016/j.devcel.2013.08.005

Zhai, B., J. Villén, S.A. Beausoleil, J. Mintseris, and S.P. Gygi. 2008. Phosphoproteome analysis of *Drosophila melanogaster* embryos. *J. Proteome Res.* 7:1675–1682. http://dx.doi.org/10.1021/pr700696a

Zhang, D., and M. Glotzer. 2015. The RhoGAP activity of CYK-4/MgcRacGAP functions non-canonically by promoting RhoA activation during cytokinesis. *eLife.* 4. http://dx.doi.org/10.7554/eLife.08898